Instabilities in the Sun-Jupiter-Asteroid Three Body Problem

John C. Urschel · Joseph R. Galante

Abstract We consider dynamics of a Sun-Jupiter-Asteroid system, and, under some simplifying assumptions, show the existence of instabilities in the motions of an asteroid. In particular, we show that an asteroid whose initial orbit is far from that of the orbit of Mars can be gradually perturbed into one that crosses Mars' orbit.

Properly formulated, the motions of the asteroid can be described as a Hamiltonian system with two degrees of freedom, with the dynamics restricted to a "large" open region of the phase space reduced to an exact area preserving map. Instabilities arise in regions where the map has no invariant curves. The method of MacKay and Percival is used to explicitly rule out the existence of these curves, and results of Mather abstractly guarantee the existence of diffusing orbits. We emphasize that finding such diffusing orbits numerically is quite difficult, and is outside the scope of this paper.

Keywords Hamiltonian Systems · Restricted Problems · Instabilities · Asteroid Belt

1 Introduction

We consider the restricted circular planar three body problem (RCP3BP) with two massive primaries, which we call the Sun and Jupiter, that perform uniform

John C. Urschel
Department of Mathematics, Penn State University
University Park, State College, PA 16802
Tel.: + 716-308-0411
Fax: + 814-865-3735
E-mail: jurschel91@gmail.com

Joseph Galante
Unaffiliated, formerly Department of Mathematics, University of Maryland
E-mail: jgalante314@gmail.com

circular motion about their center of mass. The system is normalized to mass one so the Sun has mass $1 - \mu$ and Jupiter mass μ. We further normalize so that Jupiter rotates with unit speed, resulting in a period of 2π for the primaries. The distance from the Sun to Jupiter is constant and also normalized to one. Our goal is to understand the behavior of the massless asteroid, whose position in polar coordinates is denoted by (r, ψ). It is convenient to consider the system in a rotating frame of reference which rotates with unit speed in the same direction as Jupiter. In this system, the Sun and Jupiter are fixed points on the x-axis corresponding to $\psi = 0$. We let $(r, \varphi) = (r, \psi - t)$ denote the motion of the asteroid in this rotating frame of reference. Our system has a Hamiltonian of the form:

$$H_{Polar} = H_{2BP(SA)} + \Delta H(r, \varphi) := \frac{P_r^2}{2} + \frac{P_\varphi^2}{2r^2} - P_\varphi - \frac{1}{r} + \Delta H(r, \varphi; \mu)$$

where P_r and P_φ are the momenta variables conjugate to r and φ respectively (Arnol'd et al. 2006) and ΔH is the μ-small perturbation of the associated Sun-Asteroid two body problem (2BP(SA)) by the presence of Jupiter. This system arises by initially considering the planar 3BP where the asteroid has mass m, and letting $m \to 0$. From this, we have the following equations of motion to describe the motion of our asteroid:

$$\dot{\varphi} = \frac{\partial H_{Polar}}{\partial P_\varphi} = \frac{P_\varphi}{r^2} - 1 \qquad\qquad \dot{P}_\varphi = -\frac{\partial H_{Polar}}{\partial \varphi} = -\frac{\partial \Delta H}{\partial \varphi}$$

$$\dot{r} = \frac{\partial H_{Polar}}{\partial P_r} = P_r \qquad\qquad \dot{P}_r = -\frac{\partial H_{Polar}}{\partial r} = \frac{P_\varphi^2}{r^3} - \frac{1}{r^2} - \frac{\partial \Delta H}{\partial r}$$

In addition, the RCP3BP has a conserved quantity known as the *Jacobi constant*.

$$J(r, \varphi, \dot{r}, \dot{\varphi}) = \frac{r^2}{2} + \frac{\mu}{d_J} + \frac{1 - \mu}{d_S} - \frac{\dot{r}^2 + r^2 \dot{\varphi}^2}{2} =: U(r, \varphi) - \frac{\dot{r}^2 + r^2 \dot{\varphi}^2}{2}$$

where d_J and d_S are distances from the asteroid to Jupiter and the Sun, respectively.

$$d_J(r, \varphi) = \left(r^2 - 2(1 - \mu)r \cos(\varphi) + (1 - \mu)^2\right)^{\frac{1}{2}}$$
$$d_S(r, \varphi) = \left(r^2 + 2\mu r \cos(\varphi) + \mu^2\right)^{\frac{1}{2}} \tag{1}$$

The Jacobi constant can be thought of as the total energy of our massless asteroid, with respect to our rotating frame. For a derivation of this conserved quantity, refer to sections 2.3.3 and 2.5.1 of the text by Arnol'd, Kozlov, and Neishtadt (2006).

Denote by

$$\mathcal{H}(J_0) = \{(r, \varphi) : \ U \geq J_0\}$$

a set of points on the plane of motion (configuration space). The connected components of this set are called *the Hill regions* associated with the Jacobi constant J_0. These regions are the locations in the (r, φ) plane (shaded regions in figure 6)

Fig. 1 Disjoint Hill Regions for $\mu = 10^{-3}$ and $J_0 \geq 1.52$ (Galante et at. 2011)
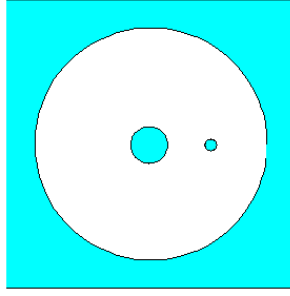
Fig. 2 Eccentricity vs. Aphelion and Perihelion Radii for $J_0 = 1.55$
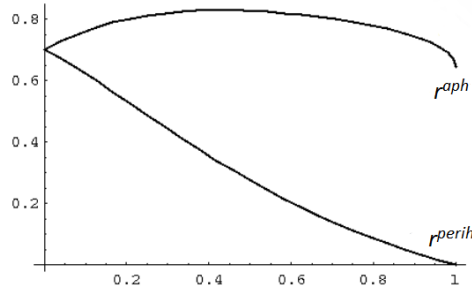
where the asteroid is allowed to move.

Fixing the Jacobi constant restricts dynamics to an invariant energy surface, denoted

$$\mathcal{S}(J_0) := \{(r, \varphi, \dot{r}, \dot{\varphi}) : J(r, \varphi, \dot{r}, \dot{\varphi}) = J_0\}$$

Most of these surfaces are smooth 3-dimensional manifolds. Let us denote by $RCP3BP(\mu, J_0)$ the RCP3BP with Sun-Jupiter mass ratio μ and dynamics restricted to the surface $\mathcal{S}(J_0)$.

For $\mu \leq 10^{-3}$ and $J_0 \geq 1.52$, the set $\mathcal{H}(J_0)$ consists of three disjoint connected components: a region around the Sun called the *inner Hill region*, a region around Jupiter called the *lunar Hill region*, and a noncompact region called the *outer Hill region*. The boundary of these regions can be found by considering the "zero velocity" curves, given by $\dot{r}^2 + r^2\dot{\varphi}^2 = 0$, which are on the boundary of the Hill regions (Arnol'd et al. 2006). In this paper, we consider only orbits contained in the inner Hill region, denoted by $\mathcal{H}^{in}(J_0)$. For convenience, denote $\mathcal{S}^{in}(J_0) = \mathcal{H}^{in}(J_0) \cap \mathcal{S}(J_0)$. When dynamics $\mathcal{S}^{in}(J_0)$ is considered, we refer exclusively to the case when the inner Hill region is disjoint from the other two.

For J_0 greater than 1.52, asteroids stay uniformly bounded away from Jupiter for all time by the energy surface constraint. However, for high eccentricities, the asteroid can make near collisions with the Sun (referred to as sun-grazers; see figure 2). A general result states that there are KAM tori near the Sun which prevent

collision (Chenciner et al. 1988).

For small μ and away from collisions, the RCP3BP is nearly integrable and can be approximated with the Sun-Asteroid two body problem (2BP(SA)), corresponding to $\mu = 0$. Elliptic motions of a 2BP have two special points where the radial velocity $\dot{r}$ of the asteroid is zero. The *perihelion* is the closest point to the Sun[1], denoted r^{perih}, and the *aphelion* is the farthest point from the Sun, denoted r^{aph}. We define the *osculating (or instantaneous) eccentricity* $e(t)$ for the RCP3BP to be the eccentricity of the asteroid in the unperturbed 2BP(SA) system, with initial conditions taken to be those of asteroid in the RCP3BP at time t.

Theorem 1 *Consider the restricted circular planar three body problem with Sun-Jupiter mass ratio $\mu = 0.001$. Fix a Jacobi Constant $J_0 = 1.55$, so that there are three disjoint Hill regions and consider dynamics in the inner Hill region. Moreover, assume that $\frac{\partial \varphi(T)}{\partial P_{\varphi_0}} > 0$ for all trajectories in a set $\Omega^{twist} \supseteq \{e \in [0.09, 0.8]\}$ which start on the surface $\Sigma = \{\dot{r} = 0, \ \ddot{r} \geq 0, \ \dot{\varphi} > 0\}$ and return to Σ after time T. Then there exist constants e^- and e^+ where $e^- \leq 0.2$ and $e^+ \geq 0.6$, and trajectories of an asteroid with initial eccentricity e^- that increase to eccentricity e^+.*

Remark: In section 2.1 we state that under these conditions, there exist orbits that become Mars crossing.

We build a mathematical framework and obtain a sufficient condition for Theorem 1 to hold. This condition guarantees applicability of so-called Aubry-Mather theory. Then we run numerical tests and evaluate the region of applicability of this theory in terms of eccentricity. Convincing numerical data shows for the Jacobi constant $J_0 = 1.55$ there existences of orbits whose eccentricity is varying from 0.2 to 0.6. For applicability of Aubry-Mather theory for the outer Hill region of the RCP3BP, refer to the works of Galante and Kaloshin (2011). For a treatment of diffusion in the Elliptic Restricted 3BP, refer to Liao and Saari (1998). In addition, for a treatment of Mars crossing orbits for the elliptic case, refer to the works of Wisdom (1982, 1983, 1985).

2 Numerical Aspects, Aubry-Mather Theory, and Regions of Instability

Let us begin to describe the mathematical framework we employ by first noting that a Jacobi energy surface is a 3-dimensional manifold. Fix $\mu \leq 10^{-3}$ and Jacobi constant $J_0 \geq 1.52$. The section $\Sigma = \{\dot{r} = 0, \ \ddot{r} \geq 0, \ \dot{\varphi} > 0\}$ is a well-defined Poincaré section in the inner Hill region. This leads to a well-defined (Poincaré)

---

[1] To be precise, the perihelion is the point where the asteroid is at the closest point to the center of mass of the system, and the Sun is within μ of the center of mass. However, in our Solar System, the radius of the Sun is approximately 0.00089 the Sun-Jupiter distance, so we allow this slight abuse in terminology for small μ.

return map on an open set Ω. One can show that Ω is homeomorphic to a 2-dimensional cylinder and can be parametrized by angle φ and conjugate momenta P_φ, or, alternatively, by φ and eccentricity $e = e(P_\varphi, J_0)$.

Suppose $\mathcal{T}^2 \subset \mathcal{S}^{in}(J_0)$ is an invariant set of the RCP3BP that is diffeomorphic to a 2-dimensional torus. Call $\mathcal{T}^2$ *rotational* if it cannot be continuously deformed inside $\mathcal{S}^{in}(J_0)$ into a closed curve or a single point. When $\mu = 0$ (i.e., when there is no perturbation), the problem reduces to the 2BP(SA) system and every such rotational 2-torus is defined by $\{e = e_0 \geq 0\}$. Bounded motions correspond to $e_0 \in [0, 1)$. In general, for e bounded away from 1 and μ sufficiently small, many of these rotational 2-tori survive due to KAM (Siegel et al. 1971). Celletti and Chierchia gave a computer assisted proof using $\mu \approx 10^{-3}$ and $J_0 \approx 1.76$ in the inner Hill region to show that near $e = 0.3$ there is a rotational 2-torus $\mathcal{T}^2$ separating $\mathcal{S}^{in}(J_0)$ into a compact "Below $\mathcal{T}^2$" component and a noncompact "Above $\mathcal{T}^2$" component (Celletti et al. 2007). We present a complementary method for a specific value of $J_0 = 1.55$; however, the method works for any $\mu \leq 10^{-3}$ and $J_0 \geq 1.52$.[2]

Define a *Region of Instability* (RI) as an open invariant set in $\mathcal{S}^{in}(J_0)$ which is homeomorphic to an annulus, and has no rotational 2-dimensional tori inside. If there is a rotational 2-torus, then it separates $\mathcal{S}^{in}(J_0)$ into "above" and "below" regions. This provides a topological obstruction to instability. To construct regions of instability, one must know about the existence of invariant curves in a given region.

Theorem 2 *In the setting of Theorem 1, the RCP3BP, restricted to the inner Hill region of a Jacobi energy surface, has a well-defined Poincaré map $\mathcal{F} : \Omega(\subset \Sigma) \to \Sigma$. Its restriction to Ω^{twist} is an exact area-preserving twist map, and there is a subregion $\Omega^{AM} \subset \Omega^{twist}$ with $[e^-, e^+] \times \mathbb{T} \subset \Omega^{AM}$, such that for any rotation number $\omega \in [\omega_-, \omega_+]$ $(\omega_\pm = \omega_\pm(e_\pm))$ there exists a corresponding Aubry-Mather set $\Sigma_\omega \subset \Omega^{twist}$ with $\Sigma_\omega \cap \Omega^{AM} \neq \emptyset$. Moreover, none of the Aubry-Mather sets Σ_ω with $\omega \in [\omega_-, \omega_+]$ are ever invariant curves.*

Abstractly, it is not clear that $e_- < e_+$ (or that $\omega_- < \omega_+$). We fix $\mu = 10^{-3}$ and $J_0 = 1.55$ for the sake of working with concrete numbers. It is shown numerically for these parameters that on the subset $\mathbb{T} \times \{e \in [0.09, 0.8]\} \subset \Omega^{twist} \subset \Omega$, the Poincaré map, denoted $\mathcal{F} = \mathcal{F}_{\mu, J_0}$, is an exact, area-preserving twist (EAPT) map. EAPT maps of this region can be studied using Aubry-Mather theory. However it is important to emphasize that Aubry-Mather (AM) theory does not apply directly as Ω may not be an invariant set. Only through a refined study of properties of $\mathcal{F}$ can it be shown that AM theory can be applied. A brief review of AM theory is found in section 6 for unfamiliar readers.

The cone crossing condition introduced by MacKay and Percival (1985) is used to obtain a sufficient condition to rule out invariant curves, as well as establish the existence of a range of Aubry-Mather invariant sets. In particular, it is used to

---

[2] For J_0 near or less than 1.52 collisions with Jupiter are hard to exclude.

establish that there are $e_{\pm}$, $e_- < e_+$ with $\mathbb{T} \times [e_-, \ e_+] \subset \Omega^{\mathrm{AM}}$. It is the set Ω^{AM} that AM theory is ultimately applied to in order to obtain the existence of orbits making large deviations in eccentricity. The cone crossing condition exploits the fact that Aubry-Mather sets are Lipschitz graphs. The MacKay-Percival sufficient condition is obtained in two steps:

– Establish bounds on the Lipschitz slope of potential invariant curves as well as Aubry-Mather sets. This gives rise to a conefield in the tangent space to Ω^{twist}, and a range of rotation numbers such that the corresponding Aubry-Mather sets are contained in Ω^{AM}.
– Show that there is a vertical strip of initial conditions such that there are tangent vectors crossing this conefield. This rules out invariant curves in Ω^{twist}.

Once a region free of invariant curves is established inside the region of twist, an application of Mather's variational method provides the existence of an orbit crossing Ω^{AM}, completing the proof of Theorem 1 (Mather et al. 1994). It is important to emphasize that the orbits in Theorem 1 are not constructed by means of numerical integration, but through abstract variational principles found in Aubry-Mather theory. Convincing numerical data is presented to obtain concrete bounds. To make the proof fully rigorous, our initial numerical tests must be verified, for example by using the machinery of interval arithmetic.

2.1 Mars crossing orbits

On $\mathcal{S}^{in}(1.55)$, an asteroid with $e = 0.2$ has radius $r \in [0.533, 0.800]$. The semi-major axis of the orbit of Mars is $\approx 1.5 AU$ and the semi-major axis of the orbit of Jupiter is $\approx 5.2 AU$ which places Mars at position $r = 0.288$ in normalized coordinates. Also on $\mathcal{S}^{in}(1.55)$, an asteroid with $e = 0.6$ has radius $r \in [0.204, 0.818]$. Thus we have the following:

Corollary 3 *Under the hypothesis of Theorem 1, there exist orbits of the asteroid which become Mars crossing.*

In the Asteroid belt there are approximately 1.7 million asteroids of radius of at least 1km. The orbits with $J_0 = 1.55$ and $e = 0.2$ are at the boundary of the main Asteroid belt. Some of them might have had significant oscillations of eccentricity as this theorem suggests. Even though an asteroid whose orbit is Mars crossing has a small chance of being captured by it (see section 2.6.2 of Arnol'd, Kozlov, and Neishtadt (2006)), enough attempts could have led to a capture. However, we stress that Mars is a not a part of our model, and, therefore, this claim cannot be completely justified by the numerics in this paper. For larger eccentricity asteroids, the perturbative effects of Mars become less negligible.

Letting Jupiter have positive eccentricity leads to the so-called Restricted Planar Elliptic Three Body Problem. This is a Hamiltonian system of two and a half degrees of freedom. It has more room for instabilities. The well-known instabilities occur in Kirkwood gaps, when the period of Jupiter and of an asteroid are

given by a rational with both numerators and denominators small, e.g. 1/3, 2/5. Mathematically, these instabilities have been recently studied by Fejoz, Guardia, Kaloshin, and Roldan (2011). For a review of diffusion in asteroid belt resonances, refer to the work of Ferraz-Mello (1999).

3 Plan of the Proof

The overall plan of our proof is as follows: we convert the dynamics to a return map, eliminate the existence of invariant curves over a section of the return map, and, finally, use existing theory to conclude that this non-existence of invariant curves results in an orbit which diffuses over the interval $[e^-, e^+]$. These three steps combined form the numerical proof of the main theorem. More explicitly, the general flow of the remainder of the paper is as follows:

Step 1: The dynamics is formulated as that of an exact area preserving twist map (EAPT) $\mathcal{F}_\mu$.

In the case $\mu = 0$, it is easy to show that $\mathcal{F}_\mu$ is a twist map. For $\mu > 0$, numerics are used to confirm this for a large region of the phase space.

Step 2: Approximate the EAPT $\mathcal{F}_\mu$ by $\mathcal{G}$.

The approximated map $\mathcal{G}$ shares the same qualitative behaviors as $\mathcal{F}_\mu$, has some desired properties that $\mathcal{F}_\mu$ lacks, and is much easier to deal with numerically. However, $\mathcal{G}$ is not guaranteed to be area preserving.

Step 3: Rule out the the presence of invariant curves for $\mathcal{G}$.

We use the aforementioned *cone crossing condition*. By design, if this condition holds for an area-preserving twist map $\mathcal{F}_\mu$ in a region Ω, then $\mathcal{F}_\mu$ has no rotational invariant curves in Ω. This condition relies on a certain conefield.

We construct a conefield for the map $\mathcal{G}$ and verify that the cone crossing condition holds for $\mathcal{G}$ in a certain region Ω. Then we show that this condition is robust and also holds for $\mathcal{F}_\mu$. This implies that $\mathcal{F}_\mu$ has no rotational invariant curves in Ω.

Step 4: Apply the Mather Connecting Theorem

We utilize the Mather Connecting Theorem and Aubry-Mather theory to conclude there exists an orbit which diffuses in the manner we prescribed.

4 Formulation of a Twist Map

Recall that motions of the asteroid in rotating polar coordinates (r, φ) can be viewed as the solutions to Hamilton's equations of motion with a Hamiltonian of

the form

$$H_{Polar} = H_{2BP(SA)} + \Delta H(r, \varphi) := \frac{P_r^2}{2} + \frac{P_\varphi^2}{2r^2} - P_\varphi - \frac{1}{r} + \Delta H(r, \varphi; \mu) \quad (2)$$

With the notations in (1), ΔH can be written

$$\Delta H := \frac{1}{r} - \frac{\mu}{d_J} - \frac{1-\mu}{d_S} = \frac{\mu(\mu-1)(1 + 3\cos(2\varphi))}{4r^3} + O(\frac{\mu}{r^4})$$

Denote the flow of the RCP3BP at time t with initial conditions $(r_0, \varphi_0, P_{r_0}, P_{\varphi_0})$ by $\Phi_t^{RCP3BP}(r_0, \varphi_0, P_{r_0}, P_{\varphi_0})$. Restricting the dynamics to the energy surface $\mathcal{S}^{in}(J_0)$ has the effect of implicitly defining one of the variables $(r, \varphi, P_r, P_\varphi)$ in terms of the other three. Further reduction of the dynamics is possible. Consider the section $\Sigma = \{\dot{r} = 0, \ \ddot{r} \geq 0, \ \dot{\varphi} > 0\}$, i.e., the perihelion surface, and take a perihelion to perihelion return map. Denote this map by $\mathcal{F}_\mu$. Let $T = T(\varphi_0, P_{\varphi_0})$ be the return time to the section. Then $\mathcal{F}_\mu(\varphi_0, P_{\varphi_0}) = (\varphi_1, P_{\varphi_1})$ is given by

$$\varphi_1 = \varphi_0 + \int_0^T \left(-1 + \frac{P_\varphi}{r^2}\right)|_{\Phi_t(\varphi_0, P_{\varphi_0})} dt$$

$$P_{\varphi_1} = P_{\varphi_0} + \int_0^T \left(-\frac{\partial \Delta H}{\partial \varphi}\right)|_{\Phi_t(\varphi_0, P_{\varphi_0})} dt$$

where the initial conditions r_0 and P_{r_0} of the flow are determined implicitly by the restriction to the energy surface $\mathcal{S}^{in}(J_0)$ and the section Σ.

A computer can be programmed to compute this map numerically. We see the output in figure 3 for $J_0 = 1.55$. Notice the apparent lack of invariant curves for $e \in [0.2, 0.6]$.

4.1 Reformulation of $\mathcal{F}_\mu$

For the two body problem there is a natural, well defined action angle coordinate system known as *Delaunay variables*, and for the RCP3BP, these coordinates are well defined for motions away from $e = 0, 1$. In short, there is a canonical transformation $\mathcal{D}(\ell, g, L, G) = (r, \varphi, P_r, P_\varphi)$ from Delaunay to polar variables. The image of $\mathcal{D}$ is only defined for bounded motions of the 2BP(SA) with $(\ell, g) \in \mathbb{T}^2$ and $0 \leq G \leq L$.

For the 2BP, L^2 is the *semi-major axis* of the ellipse of the orbit, so by Kepler's Third Law, the period $T = 2\pi L^3$. The variable $G = P_\varphi$ is the *angular momentum*, or, alternatively, LG is the *semi-minor axis* of the ellipse of the orbit. The variable $\ell \in \mathbb{T}$ is the *mean anomaly*, which is $\ell = \pi \mod 2\pi$ at the aphelion, $\ell = 0 \mod 2\pi$ at the perihelion, and, in general, $(\ell - \ell_0) = \frac{2\pi}{T} t$. The quantity $g + t$ can be interpreted as the perihelion angle (in non-rotating coordinates g itself plays this role) (Goldstein et al. 2001).

It is possible to recover the r and φ variables from Delaunay coordinates by noting that $r = L^2(1 - e\cos(u))$, where the eccentricity $e = \sqrt{1 - \frac{G^2}{L^2}}$, and u, the

Fig. 3 Return Map $\mathcal{F}_\mu$ for $J_0 = 1.55$ and $\mu = 0.001$ (φ_0 vs. eccentricity)
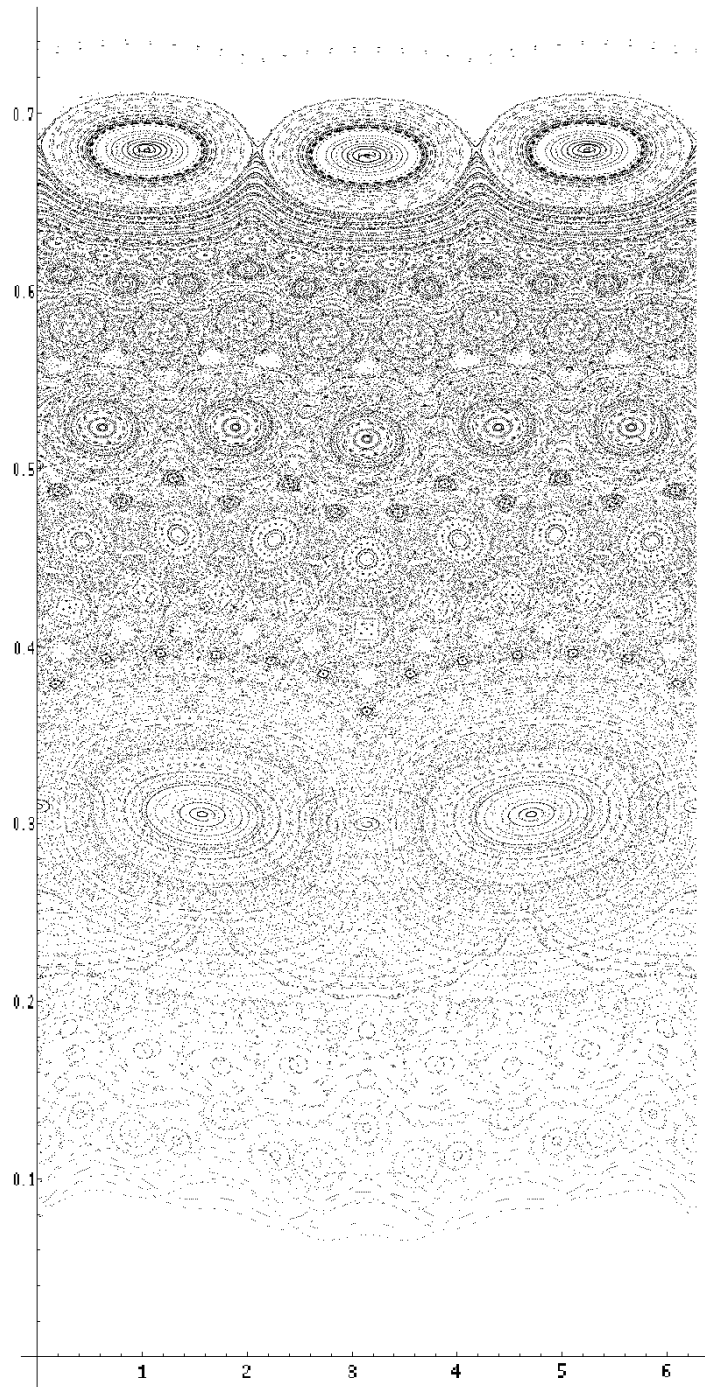
eccentric anomaly, is given implicitly by the *Kepler equation* $u - e\sin(u) = \ell$. The variable $\varphi = g + f$, where the variable f, known as the *true anomaly*, is given by $\tan\left(\frac{f}{2}\right) = \sqrt{\frac{1+e}{1-e}} \tan\left(\frac{u}{2}\right)$ or, alternatively, $r = \frac{L^2(1-e^2)}{1+ecos(f)}$.

Because the return map $\mathcal{F}_\mu$ is defined using trajectories corresponding to a full revolution of the asteroid, the variable u is periodic with period 2π. When $u = 2\pi k, k \in \mathbb{Z}$, then $f = 2\pi k$. When $\mu = 0$, there is no precession of the ellipse of orbit, i.e. $g + t$ is constant in rotating coordinates, and hence $\varphi + t = \psi$ in non-rotating coordinate is periodic. (This a restatement of the fact that the 2BP(SA) has a periodic solution, an ellipse.) Due to the 2π periodicity of the equations of motion in φ, φ_1 simplifies to $\varphi_1 = \varphi_0 + T(\varphi_0, P_{\varphi_0})$. In the 2BP(SA) case ($\mu = 0$), it holds that $T(\varphi_0, P_{\varphi_0}) = 2\pi(2J_0 - 2P_{\varphi_0})^{-3/2}$. Hence, it is possible to write in general

$$\mathcal{F}_\mu : \begin{pmatrix} \varphi_0 \\ P_{\varphi_0} \end{pmatrix} \mapsto \begin{pmatrix} \varphi_1 \\ P_{\varphi_1} \end{pmatrix} = \begin{pmatrix} \varphi_0 + 2\pi(2J_0 - 2P_{\varphi_0})^{-3/2} + \mu F_\varphi(\varphi_0, P_{\varphi_0}; \mu) \\ P_{\varphi_0} + \mu F_{P_\varphi}(\varphi_0, P_{\varphi_0}; \mu) \end{pmatrix} \quad (3)$$

where $F_\varphi(.; \mu), F_{P_\varphi}(.; \mu)$ are smooth functions in a domain bounded away from $e = 1$. We note that this map is similar in many ways to the 'Keplerian' map describing highly eccentric cometary motion as described by Broucke and Petrovsky (1987).

4.2 $\mathcal{F}_\mu$ is an EAPT

Because $\mathcal{F}_\mu$ arises as a return map of a Hamiltonian system, the map is area preserving. Additionally, due to the fact that the Hamiltonian has two degrees of freedom, the map is also exact. We claim the map is also a twist map. (See section 6 for precise definitions of exact, area preserving, and twist for an abstract map.)

We say that $\mathcal{F}_\mu$ is *a twist map* in a region Ω if

$$\frac{\partial \varphi_1}{\partial P_{\varphi_0}} > 0 \ \ \forall (\varphi_0, P_{\varphi_0}) \in \Omega$$

It is easy to see that this holds everywhere for $\mu = 0$.

Lemma 4 *The unperturbed map $\mathcal{F}_0$ is a twist map in the inner Hill Region for $J_0 > 1.5$.*

Proof: $\frac{\partial \varphi_1}{\partial P_{\varphi_0}} = 6\pi(2J_0 - 2P_{\varphi_0})^{-5/2} > 0$ since in the inner Hill region $P_{\varphi_0} < J_0$ when $J_0 > 1.5$. □

For $\mu \neq 0$, careful estimates of the perturbation terms are needed to prove twisting over a domain.[3] Let Ω^{twist} be the largest domain in Ω where the inequality $\frac{\partial \varphi_1}{\partial P_{\varphi_0}} > 0$ holds. In practice, we are only able to find a subdomain of Ω^{twist}

---

[3] Notice that the angle φ enters into the perturbation ΔH (see (2)). As the Poincaré map $\mathcal{F}_\mu$ is defined for approximately one revolution of the asteroid, then the change in the φ component should average out for higher order terms in the μ expansion of ΔH.

which is selected experimentally to be the largest domain in which the twist inequality can be proven to hold using the current best estimates on the perturbation terms. The twist property is expected to fail near $e = 1$ because of close encounters with the Sun. The map $\mathcal{F}_\mu$ is not even defined near this region because of this. Current best estimates show the following:

Claim 5 *For $\mu = 10^{-3}$ and $J_0 = 1.55$, the map $\mathcal{F}_\mu$ is a twist map in the inner Hill Region for $e \in [0.09, 0.8]$.*

Numerical Proof: A computer is used to compute the map $\mathcal{F}_\mu$. The annulus $(\varphi, P_\varphi) \in [0, 2\pi] \times [0.39, 0.83]$ is divided up into boxes of size $\frac{\pi}{16}$ by 0.01. The region $e \in [0.09, 0.8]$ corresponds to $P_\varphi \in [0.39, 0.83]$, using conservation of the Jacobi constant[4]. To compute the twist term, the partial derivative $\frac{\partial \varphi_1}{\partial P_{\varphi_0}}$ is estimated using a difference quotient with initial conditions varying by 10^{-7} in the P_φ direction. The computer finds the required inequality holds in the specified region at each grid point using this approximation. The dominant factor in the computation of the partial derivatives for twist arises from the 2BP(SA) system (see proof of Lemma 4). Because we are away from singularities at $e = 1$ (which can cause near collisions with the sun), the approximation made is acceptable and the behavior is close to that of the unperturbed system.   □

Remark: Currently this proof is verified using only numerics. To make this numerical evidence into a proof, one can use rigorous numerical integration to compute the partial derivative in question, and use interval arithmetic to make a uniform bound for each box in the annulus. This has been carried out for a few boxes in the grid using the CAPD package. Implementing rigorous numerical integration for cases when the asteroid makes a close approach to the sun requires extraordinarily good estimates on the perturbation term, meaning a high order integrator with small step size, and a very fine grid is needed. This can be quite costly in terms of computing power, and the authors were unable to show the result for every box in the grid covering the given annulus.

5 The Cone Crossing Condition

First we consider an abstract setting and then apply it to the RCP3BP. This section follows the work found in MacKay and Percival's paper (1985). Suppose $F(\theta_0, I_0) = (\theta_1, I_1)$ is an EAPT on an invariant domain Ω diffeomorphic to a cylinder $\mathbb{T} \times \mathbb{R} \ni (\theta, I)$. A (rotational) *invariant curve* $\mathcal{C} \subset \Omega$ (in this paper we study only rotational invariant curves, so we omit "rotational" for brevity) is an invariant set of F which is diffeomorphic to a circle and cannot be continuously deformed to a single point in Ω. A theorem of Birkhoff states that invariant curves are graphs over $\mathbb{T}$.

---

[4] More precisely, it follows from the geometry of ellipses that $e = \sqrt{1 - \frac{G^2}{L^2}}$ in Delauney coordinates; a quick conversion to polar coordinates yields the formula $e = \sqrt{1 - 2J_0 P_\varphi^2 + 2P_\varphi^3}$.

Theorem 6 (Birkhoff) *Suppose $\mathcal{C}$ is an invariant curve of an EAPT. Then there exists a Lipschitz continuous function P such that $\mathcal{C} \subset \{(\theta, P(\theta)) : \theta \in \mathbb{T}\}$.*

Let $D(x_1, x_2) = \frac{P(x_2) - P(x_1)}{x_2 - x_1}$, $x_1 \neq x_2$. Recall that P is Lipschitz if there exist $D^{\pm}$ such that for all x_1, x_2, $D^- \leq D(x_1, x_2) \leq D^+$.

Obtaining the Lipschitz property in Birkhoff's theorem is not hard. Simply consider the first image of the vertical line segment of height dI. It can be shown that the image of the line segment under F approximately has slope $\frac{\left(\frac{\partial I_1}{\partial I_0}\right)}{\left(\frac{\partial \theta_1}{\partial I_0}\right)}$. Taking sups over all such partial derivatives in Ω yields D^+. Doing the same for F^{-1} yields D^-. Recall, that each Aubry-Mather set is a Lipschitz graph (Mather et al. 1994). We obtain the following corollary.

Corollary 7 *Each invariant curve in Ω, at every point, has a slope inside $[D_-, D_+]$. The same is true about the Lipschitz constant for each Aubry-Mather set contained in Ω.*

Consider tangent space orbits $(F, DF) : (x, v) \mapsto (F(x), D_x F(v))$, where $x = (\theta, I) \in \mathbb{T} \times \mathbb{R}$ and $v = (\delta\theta, \delta I) \in \mathbb{T} \times \mathbb{R}$.

Theorem 8 (Cone Crossing Condition) *Suppose $\{x_i = F^i(x_0)\}$ is an orbit and $\{v_i\}$ is the tangent component to the orbit. Additionally suppose v_0 is in the upper half cone (i.e. above lines of slope $D^{\pm}$ originating at x_0), and suppose there exists an $n > 0$ so that v_n is in the lower half cone (i.e. below the lines of slope $D^{\pm}$ originating at x_n). Then the orbit does not belong to an invariant curve.*

Fig. 4 Cone Crossing Condition
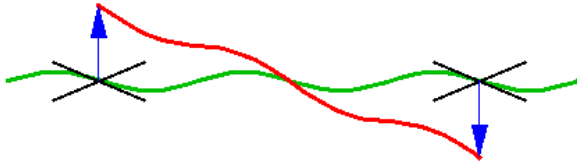
Proof: By continuity in initial conditions, a nearby orbit would cross the invariant curve. This is a contradiction (see fig. 4). □

MacKay and Percival include exposition regarding the equivalence of the cone crossing condition and action-minimizing orbits (MacKay et al. 1985). In short,

orbits which satisfy the cone crossing condition are not action-minimizing. This is because invariant curves are action-minimizing. See the associated paper for additional comments on other types of action minimizing (Aubry-Mather) sets; also see section 6.

5.1 Some preliminary numerics

In order to use the cone crossing condition in practice, tight bounds on the slopes of the cones must be obtained. It is inefficient to use the uniform upper bound on the entire phase space Ω, especially when the objects considered lay only in a smaller subset. The following algorithm attempts to rule out invariant curves by obtaining better bounds using more localized information about potentially invariant objects.

1. Input an initial condition $x_0 = (\theta_0, I_0)$ and a number of iterates n. In practice, n is chosen so that $\theta_n - \theta_0 > 2\pi$.
2. Compute a bound $\Delta I(x_0, n)$ so that $x_i = \mathcal{F}_\mu^i(x_0) \in \mathbb{T} \times [I_0 - \Delta I(x_0, n), I_0 + \Delta I(x_0, n)]$ for $i = 0, ..., n$. The interval is often referred to as a localization interval because it localizes the curve[5].
3. Compute $D^\pm$ on the annulus $\mathbb{T} \times [I_0 - \Delta I(x_0, n), I_0 + \Delta I(x_0, n)]$.
4. Use the cone crossing condition to rule out invariant curves on the annulus $\mathbb{T} \times [I_0 - \Delta I(x_0, n), I_0 + \Delta I(x_0, n)]$ using n iterates. It suffices to use the vector $(1, D^+)$ for initial conditions of the equations of variation and observe whether images in the tangent space drop below the vector $(1, D^-)$.

One does not need to apply the cone crossing condition at every point in the annulus to rule out invariant curves. It suffices to use a vertical strip in the I direction going from the bottom to the top. If all points in the vertical strip satisfy the cone crossing condition, then there are no invariant curves. (If there were, they would have have to pass through the strip by construction of ΔI.) If not all points in strip satisfy the cone crossing condition, the test to rule out invariant curves is inconclusive. In this case, a higher number of iterates may be required to rule out invariant curves, there may be point of a periodic orbit on the vertical slice, or there may be an invariant curve in the domain.

The cone crossing condition only applies to invariant domains. While all the points in the region Ω^{twist} by definition satisfy the twist property, this domain might not be invariant. By first constructing bounded regions where potential invariant curves must lay, then using the cone-crossing condition to rule out the possibility of existence invariant curves in those regions, this algorithm no longer requires invariance of the domain of twist. Instead, only the weaker condition that the localization interval remain inside in the domain of twist is required. Precise numerical estimates are required for concrete problems to ensure this condition is met. In practice this creates problems ruling out invariant curves in domains close to the boundary of Ω^{twist}, however for a sufficiently large domain of twist, there

---

[5] **This construction actually localizes all Aubry-Mather sets with rotation symbol** $\omega \in [\frac{1}{n+1}+, \frac{1}{n}-]$**. See section 6 for definitions.**

will be a sizable region where the presence of invariant curves can be ruled out.

Remarks on Application to the RCP3BP:

For $J_0 = 1.55$, $\mu = 0.001$, select $\mathbb{T} \times [0.39, 0.83] \in (\varphi, P_\varphi)^6$ to pick points from. It follows from Claim 5 that $\mathcal{F}_\mu$ is an EAPT in this domain. Step 2 of the algorithm, the construction of the localization intervals, can be estimated simply estimating the largest jump in the action component, P_φ. From the equations of motion for the RCP3BP map, this can be estimated by integrating upper bounds on the perturbation term over one revolution. A priori estimates for this are not hard to obtain and this step can be quick if one is willing to accept a larger localization interval. Step 3 can be implemented using interval arithmetic to bound domains on a vertical strip. MacKay and Percival adopted this approach, though for our purposes this is quite expensive. Step 4 requires bounds on the equations of variation.

A computer is programmed to compute the map $\mathcal{F}_\mu$ using $\mu = 0.001$ and $J_0 = 1.55$. The space $(\varphi, P_\varphi) \in [0, 2\pi] \times [0.57, 0.8]$ (corresponding to $e \in [0.2, 0.6]$) is divided up into boxes of size $\frac{\pi}{16}$ by 0.01.

To compute localization intervals, 10 iterates of the map are computed and the difference from initial conditions is measured. In this region of the phase space the size of the localization interval is no larger than 39μ. Using the localization intervals, estimates of $D^\pm$ are computed using all points in the grid. Unfortunately, the cone crossing condition is not usually satisfied using this technique. Better estimates are needed. Using either a smaller grid or better estimates on both the perturbation terms (section 7) and on the flow is a possible approach.

We pursue the method that MacKay and Percival suggested of refining estimates on the bounds $D^\pm$ and combine it with approximations specific to our map $\mathcal{F}_\mu$ to obtain the cone crossing condition. Specifically, MacKay and Percival note that the map DF induces a map on cones. Under repeated forward iterates of an initial vertical vector, the images of the vectors decrease uniformly, converging to an eigenvector of DF. Similarly for DF^{-1} (MacKay et al. 1985). This has the effect of refining the cones. Armed with sufficiently good approximations, a computer is able to estimate $D^\pm$ in each strip of size 0.01 in P_φ and find that $D^+ \leq 0.045$. Similarly, $D^- \geq -0.045$. This might suggest some type of symmetry with respect to D^+ and D^-. However, we do not assume anything of the sort. Refining at each point produces a measurable increase the bounds obtained for $D^\pm$ (4.5μ vs 39μ). However this is still not sufficient to obtain a large region with no invariant curves. Below we shall make explicit the approximations used to obtain the 4.5μ bound, and provide an additional method of refinement which shall ultimately yield our desired result.

---

[6] From hereon out, results may be stated using the (φ, P_φ) parameterization of annulus, as opposed to (φ, e). The former parameterization is easier to work with numerically; the later is better for intuition.

Remark: This method has the advantage that it does not require us to compute a fixed number of iterates n when running the algorithm to test for invariant curves. Instead, we can run a test trajectory for as long as needed to determine if the cone crossing condition is satisfied.

5.2 Some approximations

To compute the improved cones in the case of the RCP3BP, the map DF needs to be precisely computed. This is rather complicated in the case of flows (MacKay and Percival used the standard map which is cheap to compute). Let us make several approximations to $\mathcal{F}_\mu$. First, in the definition of $\mathcal{F}_\mu$, assume that $\mu F_\varphi(.;\mu) \equiv 0$. This is reasonable, as changing φ_1 by a μ small quantity over one revolution has little effect, since the φ components enter into motions only in the ΔH term, which is already μ small.

The effect of $\mu F_{P_\varphi}(.;\mu)$ is significantly more important, as it dictates how diffusion in eccentricity occurs. To compute this quantity exactly requires integration of the equations of motion for the RCP3BP, which can be computationally expensive. Instead, we use the integrable 2BP(SA) to compute this term. With the exception of high eccentricity sun grazing comets, starting from the same initial conditions, flows for the RCP3BP and for the 2BP(SA) are quite similar (in fact $O(\mu)$ close) over one revolution, so this is a reasonable approximation.

First note the following identities for the 2BP (which can be found on pg 67-68 of the text by Arnol'd, Kozlov, and Neishtadt (2006)):

$$u - e\sin(u) = L^{-3}t = \ell \qquad r = L^2\big(1 - e\cos(u)\big)$$

$$\sin(\varphi - \varphi_0) = \frac{\sin(u)\sqrt{1 - e^2}}{1 - e\cos(u)} \qquad \cos(\varphi - \varphi_0) = \frac{\cos(u) - e}{1 - e\cos(u)}$$

where φ_0 is the angle the asteroid makes with respect to the x-axis (where Jupiter is in the RCP3BP) when it is at the perihelion, i.e., when $u = 0 \mod 2\pi$ and $t = 0$. Addition formulas for sine and cosine give that

$$\sin(\varphi) = \frac{\sin(u)\sqrt{1 - e^2}}{1 - e\cos(u)}\cos(\varphi_0) + \frac{\cos(u) - e}{1 - e\cos(u)}\sin(\varphi_0)$$

$$\cos(\varphi) = \frac{\cos(u) - e}{1 - e\cos(u)}\cos(\varphi_0) - \frac{\sin(u)\sqrt{1 - e^2}}{1 - e\cos(u)}\sin(\varphi_0)$$

We make the estimate

$$\mu F_{P_\varphi}(\varphi_0, P_{\varphi_0};\mu) \approx p(\varphi_0, P_{\varphi_0};\mu) := \int_0^T -\frac{\partial \Delta H}{\partial \varphi}\big(r(t), \varphi(t)\big)|_{2BP(SA)}dt$$

$$= \int_0^{2\pi} -\frac{\partial \Delta H}{\partial \varphi}\big(r(u), \varphi(u)\big)\big(\frac{du}{dt}\big)^{-1}|_{2BP(SA)}du.$$

where φ_0 is the perihelion angle and $L_0^2 = a$ is the semi-major axis, and where the integration is performed over trajectories of the 2BP(SA). Note that for the 2BP(SA) it holds that $\left(\frac{du}{dt}\right)^{-1}|_{2BP(SA)} = Lr$. Furthermore, due to the energy surface constraint, $L = (2J_0 - 2P_{\varphi_0})^{-\frac{1}{2}}$. Refer to section 8 for an evaluation of the bounds on the error between $\mu F_{P_\varphi}(\varphi_0, P_{\varphi_0}; \mu)$ and $p(\varphi_0, P_{\varphi_0}; \mu)$. In summary, they are small enough for our purposes.

We introduce the map $\mathcal{G}$ defined by

$$\mathcal{G} := \mathcal{G}(\mu, J_0) : \begin{pmatrix} \varphi_0 \\ P_{\varphi_0} \end{pmatrix} \mapsto \begin{pmatrix} \varphi_0 + 2\pi(2J_0 - 2P_{\varphi_0})^{-3/2} \\ P_{\varphi_0} + p(\varphi_0, P_{\varphi_0}; \mu) \end{pmatrix} \tag{4}$$

The map $\mathcal{G}$ captures many of the qualitative behaviors of $\mathcal{F}_\mu$. See figure 5. The map $\mathcal{G}$ is clearly a twist map. However, $\mathcal{G}$ is not area-preserving.

Fig. 5 Approximate Return Map $\mathcal{G}$ for $J_0 = 1.55$ (φ_0 vs. eccentricity)
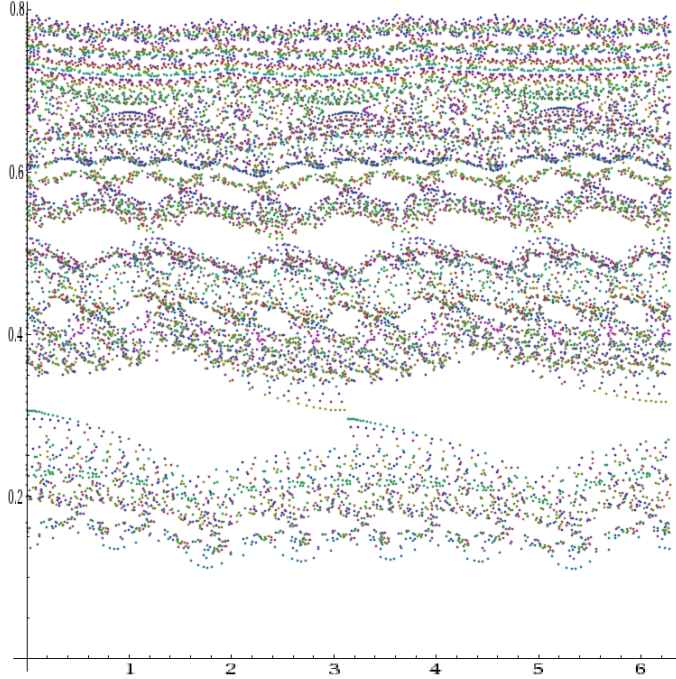
It follows that $D\mathcal{F}_\mu \approx D\mathcal{G}$, where

$$D\mathcal{G} = \begin{pmatrix} 1 & 6\pi(2J_0 - 2P_{\varphi_0})^{-5/2} \\ \frac{\partial p}{\partial \varphi_0} & 1 + \frac{\partial p}{\partial P_{\varphi_0}} \end{pmatrix}$$

Notice that knowledge of derivatives of the function $p(\varphi, P_\varphi)$ are required to compute this quantity.

$$\frac{\partial p}{\partial P_\varphi} := -\int_0^{T(P_\varphi)} \left(\left(\frac{\partial^2 \Delta H}{\partial r \partial \varphi} \right)\left(\frac{\partial r}{\partial P_\varphi} \right) + \left(\frac{\partial^2 \Delta H}{\partial \varphi^2} \right)\left(\frac{\partial \varphi}{\partial P_\varphi} \right) \right)|_{2BP(SA)} dt$$

$$- \frac{dT(P_\varphi)}{dP_\varphi} \frac{\partial \Delta H}{\partial \varphi} \left(r(T(P_\varphi)), \varphi(T(P_\varphi)) \right)$$

$$\frac{\partial p}{\partial \varphi} := \int_0^{T(P_\varphi)} -\left(\frac{\partial^2 \Delta H}{\partial \varphi^2} \right)|_{2BP(SA)} dt$$

As in the definition of $p(\varphi, P_\varphi)$ above, the integral can be expressed an integral over t, or over u, by including the appropriate Jacobian, Lr, in this case. Since only the 2BP approximation is considered, the period $T = T(P_\varphi) = \frac{\pi}{\sqrt{2}}(J_0 - P_\varphi)^{-\frac{3}{2}}$. The identities of section 4.1 imply the following:

$$\frac{\partial T(P_\varphi)}{\partial P_\varphi} = \frac{3\pi}{2\sqrt{2}}(J_0 - P_\varphi)^{-\frac{5}{2}}$$

$$\frac{\partial r}{\partial P_\varphi} = \frac{P_\varphi(P_\varphi^2 - r)}{re^2}$$

$$\frac{\partial \varphi}{\partial P_\varphi} = \frac{L\sin(u)(P_\varphi^2 + r)}{r^2 e}$$

For $\mu \neq 0$, generically $|det(D\mathcal{G})| \neq 1$, and hence the map $\mathcal{G}$ is not area preserving. However $||p||_{C^1} = O(\mu)$, so the map $\mathcal{G}$ is μ-close to the area preserving map $\mathcal{F}_\mu$. We employ the cone crossing condition on the map $\mathcal{G}$ and later offer evidence that this is sufficient to draw conclusions about $\mathcal{F}_\mu$. Doing so requires approximations of the map $\mathcal{G}^{-1}$. Computing this map precisely can be quite expensive since it typically requires shooting methods to obtain good numerics. To remedy this, consider the following *numerical* inverse of $\mathcal{G}$:

$$\mathcal{G}^{inv} := \mathcal{G}^{inv}(\mu, J_0) : \begin{pmatrix} \varphi_1 \\ P_{\varphi_1} \end{pmatrix} \mapsto \begin{pmatrix} \varphi_1 - 2\pi(2J_0 - 2(P_{\varphi_1} - p(\varphi_0^*, P_{\varphi_1}; \mu)))^{-3/2} \\ P_{\varphi_1} - p(\varphi_0^*, P_{\varphi_1}; \mu) \end{pmatrix}$$

where φ_0^* is an approximation to φ_0, given by $\varphi_0^* = \varphi_1 - 2\pi(2J_0 - 2P_{\varphi_1})^{-3/2}$.

On the region $\varphi \in [0, 2\pi]$, $P_\varphi \in [0.57, 0.8]$, numerics indicate that as defined $||\mathcal{G}^{inv} \circ \mathcal{G}(x) - x||_{C^1} < 5\mu$. Hence, the numerical inverse is μ-close to the actual inverse of the map $\mathcal{G}$.

5.3 Refined Numerics - Conefields

Definition: A *conefield* $C(X)$ is a collection $(x, v_-(x), v_+(x))$ for each $x \in X$ where $v_\pm(x) \in TX$ are vectors in the tangent space with base point x.

In the present application, the vectors in the conefield are taken to the be eigenvectors of Jacobian $D\mathcal{F}$ of the EAPT $\mathcal{F}$ at each point in the domain Ω^{twist}. MacKay and Percival (1985) proposed to iteratively refine conefields to prove the non-existence of invariant curves. The flow acts upon a conefield at a point through the action of the Jacobian matrix DF on the eigenvectors. For the RCP3BP, define the following refinements:

$$v_+^{new}(x) := \left(D\mathcal{G}\right)_{\mathcal{G}^{inv}(x)} \left[v_+\left(\mathcal{G}^{inv}(x)\right)\right] \tag{5}$$

$$v_-^{new}(x) := \left(D\mathcal{G}\right)_{\mathcal{G}(x)}^{inv} \left[v_-\left(\mathcal{G}(x)\right)\right] \tag{6}$$

Remark: Further refinements can be obtained by using higher iterates and composition.

The refinements work by flowing the eigenvectors for the map $D\mathcal{G}$ forward and backwards under the flow in the tangent space. This can be parlayed into an algorithm to refine conefields over an entire space. MacKay and Percival note that if at any point v_- lays above[7] v_+, then the interior of the cone is empty and there is no invariant curve through the phase space at that point. This can be parlayed into the following algorithm.

1. Input n, m and divide the phase space $(\varphi, P_\varphi) \in \mathbb{T} \times \mathbb{R}$ into blocks of size $1/n \times 1/m$.
2. In each block, compute bounds on the eigenvectors of $D\mathcal{G}$ and $D\mathcal{G}^{inv}$. Use these eigenvectors to define the conefield for each point in the block.
3. Use refinements 5 and 6 to refine the conefields in each block, taking upper and lower bounds where appropriate. If v_- lays above v_+, conclude there is no invariant curve inside of the block. If v_- lays below v_+, take another refinement, or alternatively, stop and leave the block as inconclusive.

A version of this algorithm is implemented. Specifically, a computer is programmed to compute the maps $\mathcal{G}$, $\mathcal{G}^{inv}$ and their derivatives, using $\mu = 0.001$ and $J_0 = 1.55$. The space $(\varphi, P_\varphi) \in [0, 2\pi] \times [0.57, 0.8]$ (corresponding to $e \in [0.2, 0.6]$) is divided up into boxes of size $\frac{\pi}{16}$ by 0.01. The initial conefields are computed using the eigenvectors. The refinement algorithm is applied to all points on the grid. This provides strong numerical evidence of the following:

Claim: For $J_0 = 1.55$, $\mu = 0.001$, $(\varphi, P_\varphi) \in [0, 2\pi] \times [0.57, 0.8]$ (corresponding to $e \in [0.2, 0.6]$) the map $\mathcal{F}_\mu$ has no invariant curves.

Numerical Proof: A computer is programmed to compute the maps $\mathcal{G}$, $\mathcal{G}^{inv}$, and their derivatives, using $\mu = 0.001$ and $J_0 = 1.55$. The space $(\varphi, P_\varphi) \in [0, 2\pi] \times [0.57, 0.8]$ (corresponding to $e \in [0.2, 0.6]$) is divided up into boxes of size $\frac{\pi}{16}$

---

[7] For $v = (a, b)$, let $\bar{v} = (1, \frac{b}{a})$ be a normalization of v. A vector v_1 lays above v_2 iff $x \geq y$, where $\bar{v}_1 = (1, x)$ and $\bar{v}_2 = (1, y)$.

by 0.01. The initial conefields are computed using the eigenvectors for $D\mathcal{G}$. The refinement algorithm given above is used for all points on the grid. Each box in the given domain requires only a finite number of iterates (an average of 15) to satisfy the cone crossing condition. Since the map $\mathcal{G}$ is μ close to $\mathcal{F}_\mu$, then the eigenvectors for $D\mathcal{G}$ are of order μ close to those of $D\mathcal{F}_\mu$. For a modest number of iterations, this difference appears to be negligible. Hence showing that the cone crossing condition holds for points in the domain using $\mathcal{G}$ implies it holds for $\mathcal{F}_\mu$ as well.   □

Remark: While this provides strong numerical evidence that there are no invariant curves for $\mathcal{F}_\mu$ in the domain $e \in [0.2, 0.6]$, the above numerical proof is not rigorous. To make it rigorous, upper and lower bounds for the cone fields and their refinements must be given for each box, not just for a representative point in the box. Interval arithmetic may be used to do this, as suggested by both Mackay and Percival (1985) and Galante and Kaloshin (2011). Alternatively, one may dispense with the map $\mathcal{G}$ entirely and compute everything using the map $\mathcal{F}_\mu$ at the cost of increased complexity in the interval arithmetic.

We have shown that $\mathcal{F}_\mu$ cannot have invariant curves in the region corresponding to $e \in [0.2, 0.6]$. This region is contained inside the twist region Ω^{twist}, however Ω^{twist} is not invariant. It is not obvious that Aubry-Mather theory can be applied to this entire non-invariant region. Abstractly, Aubry-Mather (AM) sets arise as minimizers to a variational principle. To ensure their existence, it must be shown that orbits do not stray far from the domain where the minimization is taking place. One way to see this is the case for the RCP3BP is to recall that in section 5.1, localization intervals were constructed for Aubry-Mather sets. Numerical estimates show that orbits with initial conditions inside of $\mathbb{T} \times \{e \in [0.2, 0.6]\}$ remain inside of $\mathbb{T} \times \{e \in [0.09, 0.8]\} \subset \Omega^{\text{twist}}$ after one full revolution around the sun. Independent of these concrete estimates, there are theoretical bounds which arise due to the action-minimizing properties of Aubry-Mather sets that keep the orbits we are interested in from straying too far from AM sets. These issues, along with a general review of Aubry-Mather theory is addressed in section 6. In summary, it turns out that $e \in [0.2, 0.6]$ is large enough for minimizers and connecting orbits to exist and remain bounded inside the twist region.

6 Aubry-Mather Theory

A compact invariant region C is bounded by two rotationally invariant curves C_- and C_+ such that there are no rotationally invariant curves in between C_- and C_+ is called a *Birkhoff Region of Instability* (BRI). In such BRIs, Birkhoff showed the existence of orbits coming arbitrarily close to C_- and C_+ (see the work of Mather and Forni (1994)). A much stronger result is given by Mather (1990), which allows one to specify neighborhoods of certain invariant sets which the orbit must pass through. Before stating this result, a quick overview of basic facts of Aubry-Mather theory shall be given. This review is primarily drawn from the works of Bangert (1988), Mather and Forni (1994), Gole (2001), Moser (1986),

Siburg (2004), Bourgain and Kaloshin (2005), and Xia.

Suppose $F : \mathbb{T} \times \mathbb{R} \to \mathbb{T} \times \mathbb{R}$ is a C^r $(r \geq 1)$ map. Let $\tilde{F} : \mathbb{R} \times \mathbb{R} \to \mathbb{R}$ be the lift of F to the universal cover. Let π denote the canonical projection of $\mathbb{R}$ onto $\mathbb{T}$. Call F an *exact area preserving twist map (EAPT)* if and only if

- F is area preserving: $|\det(dF)| = 1$.
- F is *exact*: For any non-contractible curve γ, the oriented area between γ and its image $F(\gamma)$ is zero.
- F is *twist*: For $\tilde{F} = (\tilde{F}_\theta, \tilde{F}_I)$ the sign of $(\partial_I \tilde{F}_\theta)$ is constant and nonzero. This implies that the image of a vertical line in the cylinder is tilted in one direction relative to the vertical direction.

Consider the bi-infinite sequence $\{\tilde{F}^i(\tilde{\theta}_0, \tilde{I}_0) = (\tilde{\theta}_i, \tilde{I}_i)\}_{i \in \mathbb{Z}}$ of images. It turns out that every EAPT can be described by a *generating function* $h : \mathbb{R} \times \mathbb{R} \to \mathbb{R}$ (Bangert 1988). This can be described via the generating function by

$$\tilde{I}_k = -\partial_1 h(\tilde{\theta}_k, \tilde{\theta}_{k+1}) \qquad\qquad \tilde{I}_{k+1} = \partial_2 h(\tilde{\theta}_k, \tilde{\theta}_{k+1})$$

The definition of h is extended to segments by

$$h(\tilde{\theta}_0, \tilde{\theta}_1, ... \tilde{\theta}_n) = \sum_{i=0}^{n-1} h(\tilde{\theta}_i, \tilde{\theta}_{i+1})$$

Definition: A segment $(\tilde{\theta}_0, \tilde{\theta}_1, ... \tilde{\theta}_n)$ is *minimizing* if for any other segment $(\tilde{\theta}'_0, \tilde{\theta}'_1, ... \tilde{\theta}'_n)$ with $\tilde{\theta}_0 = \tilde{\theta}'_0$ and $\tilde{\theta}_n = \tilde{\theta}'_n$, then

$$h(\tilde{\theta}_0, \tilde{\theta}_1, ... \tilde{\theta}_n) < h(\tilde{\theta}'_0, \tilde{\theta}'_1, ... \tilde{\theta}'_n)$$

See the work of Moser (1986) for the connection between the generating function h and the Hamiltonian. It is essentially a discrete version of the action functional, the integration of the Lagrangian dual to the Hamiltonian.

A sequence $\{\tilde{\theta}_i\}_{i \in \mathbb{Z}}$ is *minimal* if every finite segment in the sequence is minimal. Minimal sequences are action minimizing, in terms of Lagrangian formalism (Mather et al. 1994). More specifically, the generating function $h(\tilde{\theta}_0, \tilde{\theta}_1)$ gives the minimal action to move between $\tilde{\theta}_0$ and $\tilde{\theta}_1$ in one iterate of $\tilde{F}$. Notice that

$$\partial_2 h(\tilde{\theta}_{k-1}, \tilde{\theta}_k) + \partial_1 h(\tilde{\theta}_k, \tilde{\theta}_{k+1}) = 0 \text{ for all } k \in \mathbb{Z}$$

is a discrete version of the Euler-Lagrange (EL) equations. Let $\widetilde{St}(h)$ denote the set of all orbits which satisfy the discrete (EL) equations. Call such orbits *stationary orbits*. Stationary orbits are extremizers. Let $\widetilde{\Sigma}(h) \subset \widetilde{St}(h)$ denote the set of all action minimizing orbits. Note that $\widetilde{\Sigma}(h) \subset \widetilde{St}(h)$. This implies that $\pi(\widetilde{\Sigma}(h)) = \Sigma(h) \subset St(h) = \pi(\widetilde{St}(h))$. Action minimizing orbits correspond to orbits of F in the phase space (Bangert 1988, Mather et al. 1994, Xia).

For a stationary configuration $\Theta = \{\tilde{\theta}_k\}$ call the piecewise linear graph connecting $(k, \tilde{\theta}_k)$ with $(k+1, \tilde{\theta}_{k+1})$ for each $k \in \mathbb{Z}$ *the Aubry graph*. Suppose for a stationary configuration $\Theta = \{\tilde{\theta}_k\}$, the limit

$$\omega = \omega(\Theta) = \lim_{k \to \infty} \frac{\tilde{\theta}_k}{k}$$

exists. Call ω the *rotation number of* Θ. Geometrically ω is the average slope of the Aubry graph of Θ.

Theorem 9 (Aubry, Mather) *Every minimal configuration has a rotation number. Conversely, for every $\omega \in \mathbb{R}$ there is a minimal configuration with rotation number ω.*

See the work of Bangert (1988) or Mather and Forni (1994) for a proof of this fact. Note that this sheds some light onto why all Aubry-Mather sets are Lipschitz graphs.

Let $\Sigma_\omega = \{\Theta \in \Sigma(h) | \omega(\Theta) = \omega\}$ be the set of all minimal configurations of rotation number ω. This set is called an *Aubry-Mather set of rotation number ω*.

Pick a rational rotation number $\omega = \frac{p}{q}$. Let $\Sigma_{p/q}^{per}$ be the set of action minimizing periodic points of period q and rotation number p/q. Two periodic points θ^- and θ^+ are adjacent elements of $\Sigma_{p/q}^{per}$ if $\tilde{\theta}^-$ and $\tilde{\theta}^+$ have no other elements of $\widetilde{\Sigma}_{p/q}^{per}$ between them (refer to Bangert (1988) for illustrative pictures). For adjacent periodic points θ^- and θ^+ in $\Sigma_{p/q}^{per}$ let

$$\Sigma_{p/q}^+(\theta^-, \theta^+) = \{\theta \in \Sigma_{p/q} : \ \theta \text{ is backwards (resp. forwards) --asymptotic to } \theta^- \text{ (resp. } \theta^+)\}$$
$$\Sigma_{p/q}^-(\theta^-, \theta^+) = \{\theta \in \Sigma_{p/q} : \ \theta \text{ is forwards (resp. backwards) --asymptotic to } \theta^- \text{ (resp. } \theta^+)\}$$
$$\Sigma_{p/q}^\pm = \bigcup_{\theta^- \text{ adjacent to } \theta^+ \text{ in } \Sigma_{p/q}^{per}} \Sigma_{p/q}^\pm(\theta^-, \theta^+)$$

These sets are the so called heteroclinic (or homoclinic in the case of a fixed point) orbits of the periodic (resp. fixed) points.

Theorem 10 (Structure theorem: Rational case $\omega = p/q \in \mathbb{Q}$) *The Aubry-Mather set $\Sigma_{p/q}$ is a disjoint union of $\Sigma_{p/q}^{per}$, $\Sigma_{p/q}^+$, and $\Sigma_{p/q}^-$. Moreover, $\Sigma_{p/q}^{per}$ is always non-empty and if $\Sigma_{p/q}^{per}$ is not a curve, then $\Sigma_{p/q}^-$ and $\Sigma_{p/q}^+$ are non-empty as well.*

In order to distinguish such invariant sets, follow Mather and Forni (1994) and introduce rotation symbols ω^*. If Θ has an irrational rotation number ω, then its rotation symbol is $\omega^* = \omega$. In the rational case we have three options:

1. If $\Theta \in \Sigma_{p/q}^-$, then its rotation symbol is $p/q-$.
2. If $\Theta \in \Sigma_{p/q}^{per}$, then its rotation symbol is p/q.
3. If $\Theta \in \Sigma_{p/q}^+$, then its rotation symbol is $p/q+$.

There is an ordering on the set of rotation symbols given by $\omega^* < \bar{\omega}^*$ if and only if either underlying numbers satisfy $\omega < \bar{\omega}$ or $\omega = \bar{\omega} = p/q$ and $p/q- < p/q < p/q+$. This induces a topology on the space of rotation symbols (different from that on $\mathbb{R}$) (Mather et al. 1994).

It turns out that minimizers satisfy the following ordering condition:

Ordering condition: *If $\Theta = \{\tilde{\theta}_k\}$ is a minimal configuration for rotation symbol $\omega^* \leq p/q$, then $\tilde{\theta}_{k+q} \leq \tilde{\theta}_k + p$ for all $k \in \mathbb{Z}$.*

Using a sophisticated variational problem with constraints, Mather (1990) proved the following theorem about existence of connecting orbits:

Theorem 11 (Mather Connecting Theorem) *Suppose $\omega_1 < \alpha_1, \alpha_2 < \omega_2$ and suppose there are no rotationally invariant curves with rotation number $\omega \in (\omega_1, \omega_2)$ in a BRI. Then there is a trajectory in the phase space whose α-limit set lies in the Aubry-Mather set Σ_{α_1} and whose ω-limit sets lies in Σ_{α_2}. Moreover, for a sequence of rotation numbers $\{\alpha_i\}_{i \in \mathbb{Z}}$, $\alpha_i \in (\omega_1, \omega_2)$ and a sequence of positive numbers $\{\epsilon_i\}$, there exists an orbit in the phase space $\{p_j\}$ and an increasing bi-infinite sequence of integers $j(i)$ such that the $dist(\Sigma_{\alpha_i}, p_{j(i)}) < \epsilon_i$ for all $i \in \mathbb{Z}$.*

Presently there are simplifications of this proof, as well as derivations using different methodology found in the work of Bernard (2008), Bourgain and Kaloshin (2005), and Xia. It turns out that the hypothesis of a BRI in Mather Connecting Theorem can be relaxed slightly without affecting the conclusion. This is pursued in the work of Xia, §2,3. The approach is to use the so called 'barrier functions'. Let us discuss this now.

Let $\{\tilde{\theta}_k\}_{\pm k \geq 0}$ be one-sided sequences. Call a one-sided sequence action minimizing (with respect to generating function h) if every finite segment is action minimizing. There are analogous notations for one-sided rotation numbers, existence results for all one-sided rotation numbers, and structure theorems for one-sided action minimizing orbits.

Consider a sequence $\Theta_\omega^a = \{\tilde{\theta}_k^a\}_{k \in \mathbb{Z}}$ where

- $\tilde{\theta}_0 = a$
- $\{\tilde{\theta}_k\}_{k \geq 0}$ is a one-sided action minimizer with ω limit set in Σ_ω.
- $\{\tilde{\theta}_k\}_{k \leq 0}$ is a one-sided action minimizer with α limit set in Σ_ω

Consider the following *barrier function.*

$$P_\omega(a) = \lim_{N \to \infty} \left(\sum_{i=-N}^{N} h(\tilde{\theta}_k^a, \tilde{\theta}_{k+1}^a) - \inf_{\{\tilde{\theta}_{-N} \ldots \tilde{\theta}_N | \tilde{\theta}_{\pm N} = \tilde{\theta}_{\pm N}^a\}} \sum_{i=-N}^{N} h(\tilde{\theta}_k, \tilde{\theta}_{k+1}) \right)$$

It is not hard to see that for any ω, $P_\omega(a) \geq 0$ and $P_\omega(a) = 0$ if and only if there is some $\Theta \in \tilde{\Sigma}_\omega$ such that $\tilde{\theta}_0 = a$. Moreover $P_\omega(a)$ is Lipschitz continuous with respect to a, and continuous with respect to ω (in the space of rotation symbols) (Xia). It is possible to establish similar barrier functions for heteroclinic (and homoclinic) orbits to periodic orbits. In this context, the barrier function allows

one to detect the presence of an Aubry-Mather set.

A more constructive point of view is to think of barrier functions as the set up a variational problem. The solution is a constrained minimizer (the minimizer is constrained to pass through the point a). The motivates the following.

Consider two rotation numbers ω_1, ω_2 sufficiently close, an interval I, and the sequence $\Theta^a_{\omega_1,\omega_2} = \{\tilde{\theta}^a_k\}_{k\in\mathbb{Z}}$ where

— $\tilde{\theta}_0 = a \in I$
— $\{\tilde{\theta}_k\}_{k\geq 0}$ is a one-sided action minimizer with ω limit set in Σ_{ω_2}.
— $\{\tilde{\theta}_k\}_{k\leq 0}$ is a one-sided action minimizer with α limit set in Σ_{ω_1}

It is not hard to show such a sequence always exists. Consider the *joint barrier function*

$$P_{\omega_1,\omega_2}(a, I) = \lim_{N\to\infty} \left(\sum_{i=-N}^{N} h(\tilde{\theta}^a_k, \tilde{\theta}^a_{k+1}) - \inf_{\{\tilde{\theta}_{-N}...\tilde{\theta}_N \,|\, \tilde{\theta}_{\pm N} = \tilde{\theta}^a_{\pm N}, \tilde{\theta}_0 \in I\}} \sum_{i=-N}^{N} h(\tilde{\theta}_k, \tilde{\theta}_{k+1}) \right).$$

Xia proves in §3 of his paper that

Proposition 12 (Xia, Prop 3.3) *Using the above notation, let $I \subset \mathbb{R}$ be a closed finite interval and suppose $P_{\omega_1,\omega_2}(b, I) > 0$ where $b \in \partial I$. Then there exists a constrained minimizing trajectory Θ with $\tilde{\theta}_0 \in I$, with Θ forward asymptotic to a trajectory in Σ_{ω_2}, and with Θ backward asymptotic to a trajectory in Σ_{ω_1}.*

The idea of the proof is that while trajectories in the infimum are allowed to vary over all of I, the boundary condition constrains the minimizer to lie on the interior of the interval. The interval I is called a barrier for this reason. Notice that this formulation does not require a BRI operate. It only requires that there are one-sided trajectories which are asymptotic to Aubry Mather sets. The tails of the constrained minimizer limit to Aubry-Mather (AM) sets because AM sets are action minimizing and the cheapest behavior in terms of action is to follow the AM sets. In the middle, the minimizer does not vary wildly because of the constraint. Indeed, if there is a sequence Θ' which wanders too far from a small neighborhood of Σ_{ω_i}, $i = 1, 2$, then there is a cheaper trajectory which stays inside that neighborhood. There is a very strong connection to geodesics here; one can think of 'cheapest' as 'shortest' in some metric. See exposition in the works of Bangert (1988), Moser (1986), and Siburg (2004).

The neighborhood where the constrained minimizer lives may be quite small. For abstract systems, neither Xia, nor Mather give concrete bounds on the size; instead is is postulated that the rotation numbers are sufficiently close. (For a concrete system, estimation of the sizes of these neighborhoods can give some estimates on the speed of diffusion in the system). To produce general connecting orbits between any two rotation numbers, both Mather and Xia construct joint barrier functions whose constrained minimizers pass arbitrarily close to a sequence

of Aubry-Mather sets, thus establishing the Mather Connecting Theorem. Heuristically, one could think of the Aubry-Mather sets as the scaffolding upon which connecting orbits in the theorem are built.

6.1 Application to the RCP3BP

Let us now apply Aubry-Mather theory, in particular the Mather Connecting Theorem, to the RCP3BP. As mentioned, the region we consider for our analysis of the RCP3BP is **not** invariant. However the formalism above provides the existence of Aubry Mather sets inside a subset of the twist region, and allows us to construct connecting orbits in small neighborhoods of the Aubry-Mather sets. The connecting orbits won't leak outside the twist region because, by the nature of their construction, it is too expensive to do so.

Notice that the twist region Ω^{twist} defined in section 2 is not necessarily invariant; however, it is free of invariant curves. To use the Theorem 11 and the formalism defined earlier in this section, namely that connecting orbits exist in neighborhoods of AM sets, we must carefully define the neighborhoods used.

Define rotation numbers

$$\omega_{min} = \inf\{\omega : \Sigma_\omega \subset \mathbb{T} \times [0.2 \leq e \leq 0.6]\}$$
$$\omega_{max} = \sup\{\omega : \Sigma_\omega \subset \mathbb{T} \times [0.2 \leq e \leq 0.6]\}$$

to be the minimal and maximal rotation numbers, respectively, for Aubry-Mather sets which are contained in the $\mathbb{T} \times \{e \in [0.2, 0.6]\} \subset \Omega^{\text{twist}}$.

Lemma 13 *There is a continuous function $\alpha_\omega > 0$ such that for all $\omega \in [\omega_{min}, \omega_{max}]$, there is an α_ω–neighborhood of Σ_ω contained in the twist region Ω^{twist}.*

Proof: Estimates on change in angular momentum imply that making one full revolution about the Sun does not change angular momentum by more than 39μ (see numerics in section 5). Looking at the boundary of $\mathbb{T} \times \{e \in [0.2, 0.6]\}$ (corresponding to $[0.57 \leq P_\varphi \leq 0.8]$), we observe that the localization interval for solutions with initial condition $P_\varphi = 0.57$ is $P_\varphi \in [0.55, 0.58]$ and for solutions with initial condition $P_\varphi = 0.8$ is $P_\varphi \in [0.78, 0.81]$. Both of these localization intervals are contained in $P_\varphi \in [0.39, 0.83]$ (or, equivalently, $e \in [0.09, 0.8]$). Hence starting with initial eccentricity $e_0 \in [0.2, 0.6]$, the asteroid remains in the twist region $e \in [0.09, 0.8]$ after one revolution around the Sun. Therefore the Aubry-Mather sets inside of $e \in [0.09, 0.8]$ remain bounded safely inside the twist region. $\square$

Consider the collection of all such α_ω–neighborhoods. Let

$$\Omega^{\text{AM}} = \alpha(\omega_{min}, \omega_{max}) := \bigcup_{\omega \in (\omega_{min}, \omega_{max})} \alpha_\omega(\Sigma_\omega).$$

Fig. 6 Neighborhoods of Aubry Mather Sets on which connecting orbits are defined. (Galante et al. 2011)
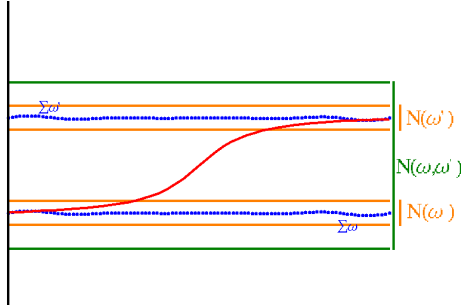
Claim: The connecting orbits found in the Mather Connecting Theorem belong to $\alpha(\omega_{min}, \omega_{max})$.

Proof: By the previous lemma, $\alpha(\omega_{min}, \omega_{max})$, and the Aubry-Mather (AM) sets contained within, are localized inside of the twist region Ω^{twist}. The connecting orbits found in the Mather Connecting Theorem thread through small neighborhoods of AM sets. AM sets are action minimizing and connecting orbits are constrained minimizers. Moving too far from a neighborhood of an AM set is cost prohibitive in terms of action. (See review of AM theory earlier in the section). Since by construction $\alpha(\omega_{min}, \omega_{max})$ is the collection all neighborhoods of AM sets with rotation number between ω_{min} and ω_{max}, then connecting orbits between these AM sets of these two rotation numbers live inside this neighborhood, and hence the twist region as well.   □

Remark: This claim, plus the application of the cone-crossing condition to the map $\mathcal{F}_\mu$, together form the proof for Theorem 2.

The lemma and subsequent claim allow us to consider dynamics only inside the region $\mathbb{T} \times \{e \in [0.2, 0.6]\}$ without having to worry about trajectories that would leak outside the region where $\mathcal{F}_\mu$ is a twist map. Essentially, trajectories which would leak outside of the twist region are too expensive too be global minimizers and are not of interest. Numerically, we have selected the region $\mathbb{T} \times \{e \in [0.2, 0.6]\}$ to be the largest such region where this is the case. Note that for different parameters μ, J_0, the region where it is possible to prove diffusion occurs using our method might be intractably small because of the problem of twist or the problem of trajectories leaking out of the twist region. While diffusion results for nearby parameters μ, J_0 are expected to be quite similar, it would be interesting to see for what parameters our approach breaks down.

Restricting to the set Ω^{AM}, where diffusion is in principle possible, it remains to setup the machinery of the Mather Connecting Theorem to deduce the existence of connecting orbits. The following lemma does this, finally establishing Theorem 1 and giving justification for Corollary 3.

Lemma 14 *There exists a trajectory which is forward asymptotic to the Aubry-Mather set $\Sigma_{\omega_{min}}$, backwards asymptotic to $\Sigma_{\omega_{max}}$, and which is contained inside the neighborhood Ω^{AM}.*

Proof: By construction $\Sigma_{\omega_{min}}$ and $\Sigma_{\omega_{max}}$ are contained inside $\Omega^{\mathrm{AM}} = \alpha(\omega_{min}, \omega_{max})$, which itself is contained inside the twist region. Furthermore, it is known that Aubry-Mather sets are ordered by rotation symbol ω, with Σ_ω and $\Sigma_{\omega'}$ close in the sense of Hausdorff distance for ω and ω' close (Bangert 1988, Mather et al. 1994). Smaller rotation numbers correspond to slower rotation around the base $\mathbb{T}$ in the φ direction. But this is to say that smaller rotation numbers correspond to higher eccentricities. By construction, ω_{min} (resp ω_{max}) is the smallest (resp largest) rotation number for Aubry-Mather sets contained in the set $\mathbb{T} \times \{e \in [0.2, 0.6]\}$ (placing $e^- \leq 0.2$, $e^+ \geq 0.6$ in Theorem 1). Hence trajectories which approach Aubry-Mather sets of these rotation numbers achieve eccentricities approaching $e = 0.2$ and $e = 0.6$. It is possible to select intermediate rotation numbers between ω_{min} and ω_{max} sufficiently close and $\{\epsilon_i\}$ sufficiently small so as to constrain minimizers to remain inside $\alpha(\omega_{min}, \omega_{max})$. (Jumps in eccentricity e are $O(\mu)$ over one revolution, so one method is to simply pick the ϵ_i and differences in rotation numbers to be $O(\mu^2)$ small.) Then by the Mather Connecting theorem, there exists an orbit with the claimed properties. $\square$

One could visualize the Aubry-Mather sets as the remainders of tori after a perturbation has been filled them with infinitely many small holes. To envision a connecting orbit, first imagine unrolling the cylinder on the real plane. A connecting orbit will be one which "climbs a set of stairs", that is, increases in the holes of the Aubry-Mather set, and then follows the remnants of a torus of higher rotation number for a while. We note that although we have proven that there exists such an orbit, that it is near quite difficult to compute such an orbit numerically.

7 Appendix: Estimates on Perturbation Terms

Recall that

$$\Delta H = \frac{1}{r} - \frac{1-\mu}{d_S(r,\varphi)} - \frac{\mu}{d_J(r,\varphi)}$$

Good approximations may be obtained by Taylor expanding $\frac{1}{r} - \frac{1-\mu}{d_S(r,\varphi)}$ in $\frac{1}{r}$ and Taylor expanding $-\frac{\mu}{d_J(r,\varphi)}$ in r about 0. Using only 4 terms in each series, it is not hard to show that for $r \in [0.1, 0.9]$, we have $|\Delta H - \Delta H^+| < 5\mu$. In fact, further away from $r = \mu$ and $r = 1 - \mu$, the difference is much smaller, closer to μ^2. For the purposes of refined numerics, very good upper bounds are required. Consider

$$\max_\varphi |\Delta H(r,\varphi;\mu)| \leq (|\Delta H|)^+(r) \qquad \max_\varphi |\partial_\varphi \Delta H(r,\varphi;\mu)| \leq (|\frac{\partial \Delta H}{\partial \varphi}|)^+(r)$$

$$\max_\varphi |\partial_r \Delta H(r,\varphi;\mu)| \leq (|\frac{\partial \Delta H}{\partial r}|)^+(r) \qquad \max_\varphi |\partial^2_{r\varphi} \Delta H(r,\varphi;\mu)| \leq (|\frac{\partial^2 \Delta H}{\partial r \partial \varphi}|)^+$$

$$\max_\varphi |\partial^2_{\varphi\varphi} \Delta H(r,\varphi;\mu)| \leq (|\frac{\partial^2 \Delta H}{\partial \varphi^2}|)^+ \qquad \max_\varphi |\partial^2_{rr} \Delta H(r,\varphi;\mu)| \leq (|\frac{\partial^2 \Delta H}{\partial r^2}|)^+$$

where

$$(|\Delta H|)^+(r) := \frac{\mu(1-\mu)}{r(r-1+\mu)(r+\mu)}$$

$$(|\frac{\partial \Delta H}{\partial \varphi}|)^+(r) := \frac{\mu(1-\mu)r\big(1+3r(r-1)+\mu(6r-3)+3\mu^2\big)}{(r-1+\mu)^3(r+\mu)^3}$$

$$(|\frac{\partial \Delta H}{\partial r}|)^+(r) := -\frac{1}{r^2} + \frac{\mu}{(r-1+\mu)^2} + \frac{1-\mu}{(r+\mu)^2}$$

$$(|\frac{\partial^2 \Delta H}{\partial r \partial \varphi}|)^+ := \mu(1-\mu)\left(\frac{3(1-\mu)}{(r-1+\mu)^4} + \frac{2}{(r-1+\mu)^3} + \frac{3\mu}{(\mu+r)^4} - \frac{2}{(\mu+r)^3}\right)$$

$$(|\frac{\partial^2 \Delta H}{\partial \varphi^2}|)^+ := 3\mu(1-\mu)\left(\frac{(1-\mu)^3}{(r-1+\mu)^5} + \frac{\mu^3}{(\mu+r)^5}\right)$$

$$(|\frac{\partial^2 \Delta H}{\partial r^2}|)^+ := -\frac{2}{r^3} + \frac{2\mu}{(r-1+\mu)^3} + \frac{2(1-\mu)}{(\mu+r)^3}$$

Remark: All of these estimates are independent of the Jacobi constant.

In the paper by Galante and Kaloshin (2011), even more explicit bounds are found for the outer region, where it suffices to expand ΔH and its derivatives entirely in terms of $\frac{1}{r}$.

8 Appendix: Difference between 2BP and RCP3BP integration for computation of $\mathcal{F}_\mu$

This appendix investigates the differences which arise from integrating over a trajectory of the 2BP(SA) vs. a trajectory of the RCP3BP in the definition of p. Suppose a flow for the RCP3BP and the 2BP(SA) start with the same initial conditions. Let $r_{3BP}(t), \varphi_{3BP}(t)$ denote the radius and angle which arise by integration of the RCP3BP and let $r_{2BP}(t), \varphi_{2BP}(t)$ denote the radius and angle which arise by integration of the 2BP(SA). Call the corresponding periods $T_{2BP} = T_{2BP}(P_\varphi)$ and $T_{3BP} = T_{3BP}(\varphi, P_\varphi)$. Then

$$\frac{\partial \Delta H}{\partial \varphi}(r_{3BP}, \varphi_{3BP}) = \frac{\partial \Delta H}{\partial \varphi}(r_{2BP} + (r_{3BP} - r_{2BP}), \varphi_{2BP} + (\varphi_{3BP} - \varphi_{2BP}))$$

$$= \frac{\partial \Delta H}{\partial \varphi}(r_{2BP}, \varphi_{2BP}) + \frac{\partial^2 \Delta H}{\partial r \partial \varphi}(\tilde{r}, \varphi_{3BP})(r_{3BP} - r_{2BP})$$

$$+ \frac{\partial^2 \Delta H}{\partial \varphi^2}(r_{3BP}, \tilde{\varphi})(\varphi_{3BP} - \varphi_{2BP})$$

where $\tilde{r} \in [r_{2BP}, r_{3BP}]$ and $\tilde{\varphi} \in [\varphi_{2BP}, \varphi_{3BP}]$.

This can be intervalized[8] as follows. Let $R = [r_{2BP}, r_{3BP}]$ and $\Phi = [\varphi_{2BP}, \varphi_{3BP}]$. The error which arises from using the 2BP(SA) vs the RCP3BP is contained in the interval

---

[8] For an introduction to interval arithmetic, refer to the paper by Wilczak and Zgliczynski (2007).

$$E := (|\frac{\partial^2 \Delta H}{\partial r \partial \varphi}|)^+ (R, \Phi) \cdot R + (|\frac{\partial^2 \Delta H}{\partial \varphi^2}|)^+ (R, \Phi) \cdot \Phi,$$

i.e.

$$\frac{\partial \Delta H}{\partial \varphi}(r_{3BP}, \varphi_{3BP}) \in \frac{\partial \Delta H}{\partial \varphi}(r_{2BP}, \varphi_{2BP}) + E.$$

E can be used to estimate the difference between $p(\varphi_0, P_{\varphi_0}; \mu)$ and $P_\varphi(t) - P_\varphi(0)$ (or, equivalently, $F_{P_\varphi}(\varphi_0, P_{\varphi_0}; \mu)$) over a revolution.

$$
\begin{aligned}
\int_0^{T_{3BP}} -(\frac{\partial \Delta H}{\partial \varphi})|_{RCP3BP} dt &= \int_0^{T_{2BP}} -(\frac{\partial \Delta H}{\partial \varphi})|_{RCP3BP} dt \\
&\quad + \int_{T_{2BP}}^{T_{3BP}} -(\frac{\partial \Delta H}{\partial \varphi})|_{RCP3BP} dt \\
&\in \int_0^{T_{2BP}} -(\frac{\partial \Delta H}{\partial \varphi})|_{2BP(SA)} dt + T_{2BP} \cdot E \\
&\quad + (T_{2BP} - T_{3BP})(|\frac{\partial \Delta H}{\partial \varphi}|)^+(R)
\end{aligned}
$$

This implies

$$|p(\varphi_0, P_{\varphi_0}; \mu) - F_{P_\varphi}(\varphi_0, P_{\varphi_0}; \mu)| \le |T_{2BP} \cdot E + (T_{2BP} - T_{3BP})(|\frac{\partial \Delta H}{\partial \varphi}|)^+(R)|.$$

A package with support for interval arithmetic can be used to compute this interval.

Consider a variational equation of the form $\delta^{i+1} = D\mathcal{G}[\delta^i]$, where δ is a two dimensional vector of the variation in each variable. From the approximating assumptions in section 5.2, and the interval enclosure above, the initial variation from φ is negligible, and the variation from P_φ is bounded by $|T_{2BP} \cdot E + (T_{2BP} - T_{3BP})(|\frac{\partial \Delta H}{\partial \varphi}|)^+(R)|$. This gives a bound of the overall difference between using $\mathcal{G}$ and $\mathcal{F}_\mu$, per iteration.

9 Appendix: Software Used For Numerics

The numerics found in this paper are of two distinct varieties: rigorous numerics involving interval arithmetic, and nonrigorous numerics making use of floating point arithmetic. Whenever possible, interval arithmetic is used to obtain results. Interval arithmetic has the advantage of being validated. The computer actually proves the result. This is why pains were taken in section 8 to set up statements in terms of interval enclosures. Mathematica supports interval arithmetic, as does the popular CAPD package for rigorous numerical integration. Unfortunately interval arithmetic can be very time consuming (the results in Galante and Kaloshin's paper (2011) took hundreds of days of computer time), so the authors needed to

resort to nonrigorous floating point arithmetic. When used, precision is lost and results can only be stated in terms of $big - O$ notation in some cases, which is why many things are stated being $O(\mu)$ close. Mathematica was used to produce such results because it was relatively quick to implement routines to check the claims made. The instances of floating point arithmetic where a finite term of size $O(\mu)$ is bounded or evaluated are generally believed to be very accurate since the errors the computer makes are of order 10^{-16}, compared to 10^{-3}.

The instances of floating point arithmetic involving numerical integration over short periods of time (on average, 15 revolutions) are believed to be accurate, as they arose from instructing Mathematica to use step sizes of approximately 10^{-16}. Mathematica internally uses an adaptive Runge-Kutta integrator. General theory says the error for short time periods of integration will be $O(10^{-15})$. Exactly what constitutes a "short time period" in a chaotic system is highly dependent on the system and it has been shown that nonrigorous RK integrators fail to accurately model chaotic flows for longer periods of time. This spurred the creation of rigorous numerical integrators such as the CAPD described by Wilczak and Zgliczynski (2007). The paper is setup so that when sufficient computing power becomes available, the dedicated reader may convert the floating point results to interval arithmetic results and fully validate all the claims presented.

The code used for the computations involved in this paper, can be found online on the webpage http://www.personal.psu.edu/jcu5018/, under the publications tab. The Mathematica notebook involved with this paper is entitled instabilities_in_the_ asteroid_belt.nb. In addition to this notebook, there is a larger notebook, entitled RCP3BP_estimates_4v4.nb, created by the authors, which contains a collection of various functions for the RCP3BP in both rotating polar and Delaunay coordinates. The functions in this notebook are required to effectively run the associated code for this paper. The notebook instabilities_in_the_asteroid_belt.nb contains notes within it to help understand what is occuring at each step. Below, we will give a detailed analysis of the numerical aspect of the paper. The main functions of the notebook are as follows:

- define the return map $\mathcal{F}_\mu$
- verify twist in the region $e \in [0.09, 0.8]$ for $\mathcal{F}_\mu$
- define the approximation function $p(\varphi_0, P_{\varphi_0}; \mu)$
- define both the approximation map $\mathcal{G}$, and its approximate numerical inverse $\mathcal{G}^{inv}$
- verify that the approximate numerical inverse $\mathcal{G}^{inv}$ is an acceptable inverse
- obtain bounds on $D^{\pm}$ for each grid point of $\mathbb{T} \times [0.39, 0.83] \in (\varphi, P_\varphi)$
- implement MacKay and Percival's cone crossing condition on $\mathcal{G}$
- output an array, verifying that the cone crossing conditon holds for each grid point of $\mathbb{T} \times [0.39, 0.83] \in (\varphi, P_\varphi)$

We detail the numerical technique used for each of these steps.

The return map is defined, through a semi-iterative procedure. We begin by defining a function $ReturnTime$, that finds the time it takes to make k orbits from perihelion to perihelion. This is done by using the 2BP period $T = 2\pi L^3$ as an initial guess, and searching for the closest solution of $P_r = 0$ to our initial guess us-

ing root finding (Mathematica internally implements some variant of the Newton's method for this). Through experimentation, we find that for larger values of k, the initial guess loses accuracy (the original 2BP estimate of the period no longer holds), and may result in a return time to an apohelion (also on $P_r = 0$). The guesses have been numerically tested to accurately give perihelion to perihelion return times for pieces of orbit 3 revolutions long. For this reason, the return map is defined to run iteratively, using jumps of $k = 3$, where the initial guesses for the return times are reset using end coordinates, after which the map is stepped in single iterates to reach the desired return map iteration.

To verify twist in a region it suffices to compute $\frac{dT}{dP_{\varphi_0}} > 0$.

Claim: $\frac{dT}{dP_{\varphi_0}} > 0$ in a given region implies that region is twisting.

Proof: The chain rule implies that $\frac{d\varphi_1}{dP_{\varphi_0}} = \frac{d\varphi_1}{dT}\frac{dT}{dP_{\varphi_0}}$. To see that $\frac{d\varphi_1}{dT} > 0$, recall the integral equation $\varphi_1 = \varphi_0 + \int_0^T \left(-1 + \frac{P_\varphi}{r^2}\right)|_{\Phi_t(\varphi_0, P_{\varphi_0})}dt$ and note that $\dot\varphi = -1 + \frac{P_\varphi}{r^2} > 0$. $\qquad\square$

To show twist in the region $P_\varphi \in [0.39, 0.83]$ (or $e \in [0.09, 0.8]$), a grid of solutions of size $\frac{\pi}{16}$ by 0.01 is generated. At each grid point (φ, P_φ), $ReturnTime$ at (φ, P_φ) and $(\varphi, P_\varphi + 10^{-7})$ is computed. It turns out $ReturnTime_{(\varphi, P_\varphi + 10^{-7})} - ReturnTime_{(\varphi, P_\varphi)} > 0$ for all (φ, P_φ) in this region. In fact, we find the minimum value of $ReturnTime_{(\varphi, P_\varphi + 10^{-7})} - ReturnTime_{(\varphi, P_\varphi)}$ on this grid to be 1.95. Using a difference quotient with difference 10^{-7} in the P_φ direction to approximate $\frac{dT}{dP_{\varphi_0}}$ provides strong evidence for $\frac{dT}{dP_{\varphi_0}} > 0$, and thus for twist. To rigorously prove twist would require replacing the evaluations at grid points with bounds on intervals, and replacing the difference quotient with the equations of variation.

We move on to the approximating function p. The definition of the function $p(\varphi_0, P_{\varphi_0}; \mu)$ is straightforward. Recall, from section 5.2, that

$$p(\varphi_0, P_{\varphi_0}; \mu) = \int_0^{2\pi} -\frac{\partial \Delta H}{\partial \varphi}\left(r(u), \varphi(u)\right)\left(\frac{du}{dt}\right)^{-1}|_{2BP(SA)}du.$$

$p(\varphi_0, P_{\varphi_0}; \mu)$ is computed by numerical integration. $\frac{\partial p}{\partial \varphi}$ and $\frac{\partial p}{\partial P_\varphi}$ are computed in a similar fashion (refer to section 5.2 for their definitions). The derivatives $\frac{\partial p}{\partial \varphi}$ and $\frac{\partial p}{\partial P_\varphi}$ become of use when calculating $D\mathcal{G}$ and $(D\mathcal{G})^{inv}$.

Defining the approximation map $\mathcal{G}$ and the approximate numerical inverse map $\mathcal{G}^{inv}$ is a matter of numerically implementing the map definition found in section 5.2. To verify that $\mathcal{G}^{inv}$ is an appropriate numerical inverse, we take a grid of size $\frac{\pi}{16}$ by 0.01 for $\mathbb{T} \times [0.39, 0.83]$. At each grid point, the map $\mathcal{G}^{inv} \circ \mathcal{G}$ is computed. Comparing the original point $x = (\varphi_0, P_{\varphi_0})$, and the result $\mathcal{G}^{inv} \circ \mathcal{G}(x)$ componentwise at each grid point, we find the largest difference to be 3.18×10^{-3}. From this, one can infer that $||\mathcal{G}^{inv} \circ \mathcal{G}(x) - x||_{C^1} < 5\mu$ for the region $\varphi \in [0, 2\pi]$, $P_\varphi \in [0.57, 0.8]$ and accept $\mathcal{G}^{inv}$ as an acceptable numerical inverse.

The cone values $D^{\pm}$ are calculated at each grid point $(\varphi_0, P_{\varphi_0})$ by computing the eigenvectors of $D\mathcal{G}$ and $D\mathcal{G}^{inv}$, respectively, and taking the cone value at each point to be the largest magnitude eigenvector in the localization interval of P_{φ_0}. When it comes to the actual cone crossing condition, the algorithm is straightforward. For each grid point $x_{\pm,0} = (\varphi_0, P_{\varphi_0})$, we take the initial condition $v_{\pm,0}$ to be $(1, \delta P_{\varphi_0})$ and apply the following iteration at each step:

$$x_+ = \mathcal{G}(x_+) \qquad\qquad v_+ = D\mathcal{G}(x_-)v_+$$
$$x_- = \mathcal{G}^{inv}(x_-) \qquad\qquad v_- = D\mathcal{G}^{inv}(x_+)v_-$$

This follows from (7.1) and (7.2) of MacKay and Percival's paper (1985). At each iteration, check if $v_- > v_+$ (meaning that, when normalized, for $v_{+,N} = (1, y)$ and $v_{-,N} = (1, z)$, it holds that $z > y$). If this occurs at a given iteration, we record the step, terminate the loop, and can conclude that the cone-crossing condition has been satisfied at that grid point. An array is constructed detailing the number for which this occurs at each grid point. On average, this requires approximately 15 steps for the cone crossing condition to be satisfied. In some very rare cases, a grid point may require over 100 iterations. Taking too many iterates at a grid point relies on the computer's ability to perform long term numerical integration.

Although we satisfy the cone crossing condition over the entire grid in our region, in practice, all that is required is to satisfy the condition for the boundary $P_{\varphi}^- = P_{\varphi}^-(e_-)$, $P_{\varphi}^+ = P_{\varphi}^+(e_+)$ of our region, and an arbitrary vertical slice $[P_{\varphi}^-, P_{\varphi}^+] \times \{\Delta\varphi\} \subset \Omega$. As discussed by MacKay and Percival (1985), to prove the non-existence of rotational invariant curves, it suffices to consider a vertical slice. The main difference is that in their paper, they are examining their entire map (the standard map), whereas we are considering a subset of ours. For this reason, we must satisfy the cone-crossing condition at the boundary $P_{\varphi}^- = P_{\varphi}^-(e_-)$ and $P_{\varphi}^+ = P_{\varphi}^+(e_+)$. This gives us a certain leeway regarding the high number of iterates required for a select number of grid points. Based on the numerical results given by our notebook, we have given strong numerical evidence for the non-existence of invariant curves for $e \in [0.2, 0.6]$.

References

1. Arnol'd, Vladimir; Kozlov, Valery; Neishtadt, Anatoly. *I. Mathematical aspects of classical and celestial mechanics.* Dynamical systems. III. Translated from the Russian original by E. Khukhro. Third edition. Encyclopaedia of Mathematical Sciences, 3. Springer-Verlag, Berlin (2006)
2. Bangert, Victor. *Mather sets for twist maps and geodesics on tori.* Dynamics reported, Vol. 1, 1–56, Dynam. Report. Ser. Dynam. Systems Appl., 1, Wiley, Chichester (1988)
3. Bernard, P. *The Dynamics of Pseudographs in Convex Hamiltonian Systems,* J. Amer. Math. Soc. 21 (2008), no. 3, 615–669.
4. Bourgain, Jean, Kaloshin, Vadim. *On diffusion in high-dimensional Hamiltonian systems.* J. Funct. Anal. 229 (2005), no. 1, 1–61.

5. Broucke, Roger; Petrovsky, Tomio. *Area-preserving mappings and deterministic chaos for nearly parabolic motions.* Celestial Mech. 42, no. 1-4, 53–79 (1987)

6. Curtis, Howard. *Orbital Mechanics for Engineering Students.* Second Edition. Butterworth-Heinnemann, Amsterdam (2010)

7. Celletti, Alessandra; Chierchia, Luigi. *KAM stability and celestial mechanics.* Mem. Amer. Math. Soc. 187, no. 878, viii+134 (2007)

8. Chenciner, Alain; Llibre, Jaume. *A note on the existence of invariant punctured tori in the planar circular restricted three-body problem.* Ergod. Theor. Dyn. 8, 63-72 (1988)

9. Fejoz, Jacques. *Quasiperiodic Motions in the Planar Three-Body Problem.* Journal of Differential Equations Vol 183, Issue 2, 303-341 (2002)

10. Fejoz, Jacques; Guardia, Marcel; Kaloshin, Vadim; Roldan, Pablo. *Diffusion along mean motion resonance in the restricted planar three-body problem.* arXiv:1109.2892v1 (2011)

11. Ferraz-Mello, Sylvio. *Slow and Fast Diffusion in Asteroid-Belt Resonances: A Review* Cel. Mech. Dyn. Ast. 73, 25 (1999)

12. Gole, Christopher. *Symplectic twist maps. Global variational techniques.* Advanced Series in Nonlinear Dynamics, 18. World Scientific Publishing Co., Inc., River Edge, NJ, xviii+305 pp. (2001) ISBN: 981-02-0589-9

13. Galante, Joseph; Kaloshin, Vadim. *Destruction of Invariant Curves in the Restricted Circular Planar Three Body Problem Using Comparison of Action.* Duke Math J, vol. 159, no. 2, 275-327 (2011)

14. Galante, Joseph; Kaloshin, Vadim. *Construction of a Twisting Coordinate System for the Restricted Circular Planar Three Body Problem.* Manuscript. Available at http://www.terpconnect.umd.edu/ vkaloshi/papers/Twist-spreading-Joseph.pdf

15. Galante, Joseph; Kaloshin, Vadim. *Destruction of Invariant Curves in the Restricted Circular Planar Three Body Problem Using Ordering Condition.* Manuscript. Avaliable at http://www.terpconnect.umd.edu/ vkaloshi/papers/localization-joseph.pdf

16. Goldstein, Herbert; Poole, Charles; Safko, John. *Classical Mechanics.* Third edition. Addison Wesley, San Francisco (2001)

17. Kaloshin, Vadim. *Geometric Proof of Mather's Connecting Theorem.* Preprint. Available Online. http://www.its.caltech.edu/ kaloshin/research/mather.pdf

18. Liao, Xinhao; Saari, Donald G. *Instability and Diffusion in the Elliptic Restricted Three-body Problem* Celestial Mechanics and Dynamical Astronomy. Volume 70, Number 1, 23-39 (1998)

19. MacKay, Robert; Percival, Ian. *Converse KAM.* Comm. Math. Phys. Volume 98, Number 4, 469-512 (1985)

20. Mather, John. *Variational construction of orbits of twist diffeomorphisms.* J. Amer. Math. Soc. 4, no. 2, 207-263 (1991)

21. Mather, John. *Differentiability of the minimal average action as a function of the rotation number.* Bo. Soc. Bras. Mat., 21, 59-70 (1990)

22. Mather, John; Forni, Giovanni *Action minimizing orbits in Hamiltonian systems.* Transition to chaos in classical and quantum mechanics (Montecatini Terme, 1991), 92–186, Lecture Notes in Math., 1589, Springer, Berlin (1994)

23. Moser, Jurgen. *Recent Development in the Theory of Hamiltonian Systems.* SIAM Review. Vol 28, No 4. 459-485 (1986)

24. Moser, Jurgen. *Stable and random motions in dynamical systems.* With special emphasis on celestial mechanics. Reprint of the 1973 original. With a foreword by Philip J. Holmes. Princeton Landmarks in Mathematics. Princeton University Press, Princeton, NJ (2001)

25. Rogel, J. V. *Early Aubry-Mather theory.* Informal talks delivered at the Summer colloquium of the Computational Science Department at the National University of Singapore (2001).

26. Siburg, Karl Friedrich. *The principle of least action in geometry and dynamics.* Lecture Notes in Mathematics, Springer-Verlag, Berlin, xii+128 pp. (2004) ISBN: 3-540-21944-7

27. Siegel, Carl; Moser, Jurgen. *Lectures on celestial mechanics.* Translation by Charles I. Kalme. Die Grundlehren der mathematischen Wissenschaften, Band 187. Springer-Verlag, New York-Heidelberg (1971)

28. Wisdom, Jack. *The origin of the Kirkwood Gaps* Astron. J. 87, 577-593 (1982)

29. Wisdom, Jack. *Chaotic Behavior and the Origin of the 3/1 Kirkwood Gap* Icarus 56, 51-74 (1983)

30. Wisdom, Jack *A Pertubative Treatment of motion Near the 3/1 Commensurability* Icarus 63, 272-289 (1985)

31. Wilczak, Daniel; Zgliczynski, Piotr. *The C^r Lohner-algorithm.* arXiv:0704.0720v1 (2007)

32. Xia, Jeff. *Arnold Diffusion and Instabilities in Hamiltonian Systems.* Preprint. Available Online. http://www.math.northwestern.edu/ xia/preprint/arndiff.ps